IMPROVEMENT IN DESIGN OF CENTRIFUGAL SLURRY PUMP USING CFD

Thesis submitted in partial fulfillment of the requirements for the award of the degree of

MASTER OF ENGINEERING

IN

THERMAL ENGINEERING

Submitted by:

MITESH KUMAR
Registration no.: 801183013

Under the Guidance of

Mr. Satish Kumar
Assistant Professor
Mechanical Engineering Department
Thapar University, Patiala.

Dr. S.K. Mohapatra
Senior Professor & DOAA
Mechanical Engineering Department
Thapar University, Patiala.

MECHANICAL ENGINEERING DEPARTMENT
THAPAR UNIVERSITY
PATIALA-147004, INDIA.
July 2013

DECLARATION

DECLARATION

I hereby declare that the work which is being presented in the dissertation entitled, **"IMPROVEMENT IN DESIGN OF CENTRIFUGAL SLURRY PUMP USING CFD"** in partial fulfillment of the requirements for the award of the degree of Master of Engineering in Mechanical Engineering with specialization in **THERMAL ENGINEERING** submitted in **Mechanical Engineering Department** of Thapar University, Patiala, is an authentic record of my own work carried out under the supervision of Mr. Satish Kumar and Dr. S.K. Mohapatra. The work refers other researchers' works which are duly listed in the references section.

The matter presented in this thesis has not been submitted for the award of any other degree of this or any other university.

Mitesh Kumar

Date: 15-7-13

Place: Patiala

Mitesh Kumar
(801183013)

This is to certify that the above statement made by the candidate is correct and true to the best of our knowledge.

Supervisors

Mr. Satish Kumar
Assistant Professor,
Thapar University, Patiala

Dr. S.K. Mohapatra
DOAA & Senior Professor
Thapar University, Patiala

Countersigned by

Dr. Ajay Batish
Professor & Head of Department
Mechanical Engineering Department
Thapar University, Patiala

Dr. S.K. Mohapatra
Dean of Academic Affairs
Thapar University, Patiala

ACKNOWLEDGEMENT

I would like to show my gratitude and indebtness to my research supervisor Mr. Satish Kumar, Assistant Professor, Mechanical Engineering Department, Thapar University, Patiala for his invaluable guidance and suggestions which inspired me to submit thesis report in the present form.

I would like to express my deepest respect towards my co-supervisor, Dr. S.K. Mohapatra, Senior Professor & Dean of Academic Affairs, Thapar University, Patiala for guiding and inspiring me in the course of the research work. The fruitful discussions with him throughout the research work were a great help for the successful completion of the present work.

It is a great pleasure to thank the authorities of Thapar University, Patiala for providing this opportunity to carry out my reseacrh work successfully.

I owe sincere and earnest thankfulness to my family members who enthused, encouraged and fully supported me for every trial that comes my way. They did not supported just financially, but also morally and spiritually.

I acknowledge my sincere thanks to all my friends and classmates for providing the companionship and making my stay at Thapar University, Patiala pleasant and joyful.

Last but not the least, To God the father of all, I thank for the strength that keeps me standing and for the hope that keeps me believing that this affiliation would be possible and more interesting.

Mitesh Kumar

ABSTRACT

The present study on the improvement in design of centrifugal slurry pump was conducted at the Mechanical Engineering Department, Thapar University, Patiala. Centrifugal slurry pumps have been widely used for slurry transportation in thermal power plants, chemical process plants, sewage pumping etc. Computational Fluid Dynamics (CFD) has become more popular approach for designing and performance evaluation of such complex machines. In the present work numerical simulations for centrifugal slurry pump were performed in order to give design improvements to the existing design of the pump. Numerical simulations were performed using Eulerian model with CFD package, ANSYS Fluent 6.3.26. The geometry generation of the different designs of pump were done using Gambit 2.3.16. The turbulence in the liquid phase has been described using k-ε model. The multiphase physics has been described using mixture model.

Visualization of previous results from numerical simulations on the same pump has been done in order to find drawbacks in design. Two regions, namely, cutwater region and volute tongue region, were found for the geometry improvement. Four different models were prepared by assigning the design improvements to these regions. Numerical analysis of these models was done to find the most suitable design. After, visualizing the numerical results and Head trends for these models, model with straight tongue and rounded cutwater was found to be the best design.

Moreover, another design parameter: number of blades, was also considered to improve the design. Two new models with blade number 4 and 6 were produced and analyzed numerically with single phase. However, numerical results revealed that higher number of blades should also be considered to optimize the number of blades.

LIST OF FIGURES

LIST OF TABLES

Notations

α_k	:volume fraction of the k^{th} phase
Γ_k	:rate of mass generation of phase k at interface
ρ_k	:density of the k^{th} phase
$\vec{v}_k$	:velocity of k^{th} phase
$\vec{v}_m$	:velocity of mixture
ρ_m	:density of mixture
c_k	:mass fraction of k^{th} phase
M_k	:average interfacial momentum source for the phase k
τ_k	:average viscous stress tensor
τ_{Tk}	:turbulent stress tensor
$\vec{v}_{Mk}$	:diffusion velocity
τ_m	:stress tensor for mixture.
μ_t	:turbulence viscosity
k	:turbulence kinetic energy
ω	:turbulence frequency
ρ	:density of phase
$\vec{v}$	:absolute velocity
$\bar{\bar{\tau}}$	:stress tensor
$\vec{g}$	:acceleration due to gravity
p	:pressure
k	:thermal conductivity
φ	:dissipation
S_i	:heat generation
T	:terminal Energy per unit volume
V_d	:velocity of fluid in delivery pipe (m/s)

V_s	:velocity of fluid in suction pipe (m/s)
Z_d is	:delivery head (meters)
Z_s	:Suction lift (meters)
Q	:flow rate, m^3/s
$(\frac{P_d}{\rho g})$	:Delivery pressure gauge reading delivery side (m)
$(\frac{P_s}{\rho g})$	:Vacuum gauge reading at suction side (m)

CHAPTER 1 INTRODUCTION

1.1 PUMPS AND CLASSIFICATIONS

Pumps are mechanical devices, which uses suction or pressure to transfer fluids from one place to another. Pumps have two main purposes:

- Liquid transfer from a place to another (e.g. water from a well to the water tank at some other place)

- Circulate liquid inside a system (e.g. cooling water or lubricants through machines and equipment)

Pumps have a variety of applications and it comes in different sizes according of applications. Pumps can be classified into various types on basis of their working principle

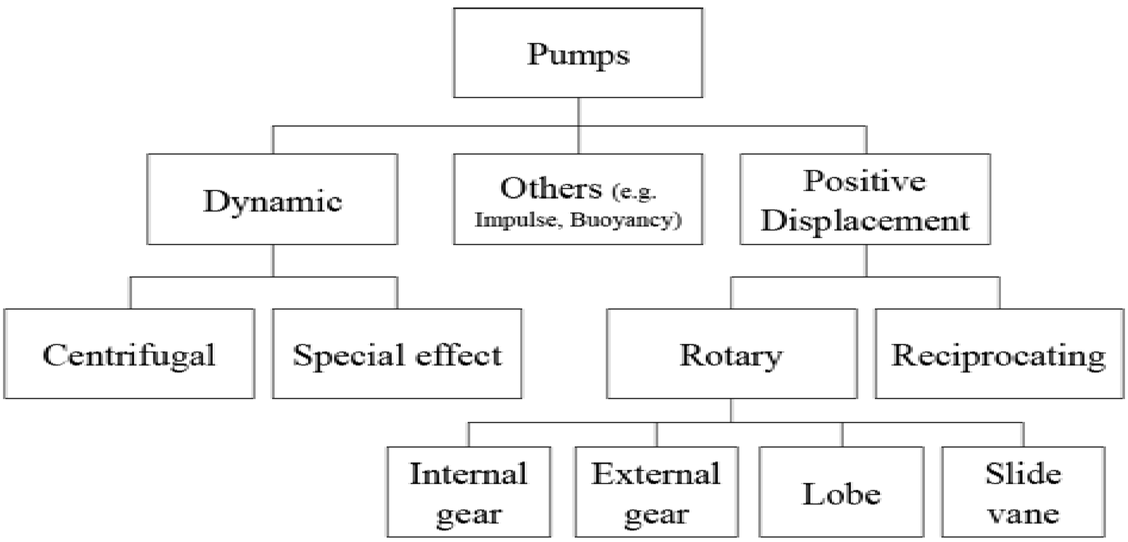

Figure 1.1: Classification of Pumps

1.2 BASIC SLURRY TRANSPORTATION SYSTEM

There are several means for the transportation of solids. They can be transported either pneumatically or hydraulically. Pneumatic and Hydraulic mode of transfer differ from each other on the basis of the types of fluid they use to transfer and also the nature of suspension of the solid particles in different continuum media. Solids are first mixed and then transported to the destination for utilization. There are different slurry transportation systems available for different types of materials according as their end requirements

Slurry transportation systems can be systems classified into three sub-systems namely: -

1. Slurry preparation facility.
2. Main pipeline and pumps
3. Terminal facility

1.3 ASH DISPOSAL USING CENTRIFUGAL PUMP

The selection of slurry pumps mainly depends on the practical considerations rather than the economical concerns of efficiency. However, the pressure discharge and the abrasivity are the two important factors for the selection of a pump. Lots of different types of pumping systems are used for slurry transportation purposes. Positive displacement and special effect pumps are used but so far the most important and common type of slurry pump is the centrifugal slurry pump. The centrifugal slurry pump uses the centrifugal force generated by the rotating motion of the impeller to provide kinetic energy to the slurry. The selection of centrifugal slurry pumps mainly depends on impeller size, passage design, shaft seal possibilities and materials. The wear caused by the abrasive attack on the wetted materials, is one of the important factor an application engineer should consider before selecting the slurry pumping system.

Slurry pumps are accustomed to transport abrasive and high concentration suspension in several industries such as: Gold, Silver, iron ore, Lead & Zn, sands, Tin, Steel, Titanium, Molybdenum, Copper, electrical Utilities, Oil Shale, Water & sewerage Utilities, Coal, Sand & Gravel, Tobacco, Agriculture etc.

Slurry pumps are used widely in the mining industry where most plants use wet separation systems. These slurry pumps usually move large volumes of slurry for different processes. Slurry pumps are also used for the ash disposal in the thermal power plants. Increased world concerns on the atmosphere and energy consumption will definitely generate a lot of wider uses for slurry pumping in years to come.

Determining whether to use the centrifugal pump for slurry transportation is a challenging decision. Usually, slurry pump costs many times than a standard water pump and this make the use of slurry pump very difficult. One of the main problems in selecting a pump is deciding whether or not the fluid to be pumped is actually slurry or not. We can define slurry as any solid-fluid mixture that contains more solids than that of drinking or ground water. Again, this does not mean that a slurry pump must be used every time where there is a trace of solid particles, but at least a slurry pump should be considered.

1.4 GENERAL INFORMATION ON CFD ANALYSES OF THE PUMPS

The main application of CFD to the pumps is in the computation of the pump characteristics. There are two main methodology found applicable to the pump applications while simulating the motion of the rotor. The first one is the frozen rotor model in which the frame of reference is moved rather than the element which is actually moving in the practical system.

A frame of reference is employed on the moving element and other frame of reference is employed at some stationary point. The two frames of reference connect in such a way that they each have a fixed relative position throughout the calculation, but with the appropriate frame transformation occurring across the interface. There are two main disadvantages of frozen rotor model. The first disadvantage is caused by not modeling the transient effects at the frame change interface and the second one is the losses occurred in transient case as the flow is mixed between the rotating and stationary components. The second methodology used for simulating the motion of the rotor is the transient rotor-stator model. In this model, the transient motion of the rotor is simulated within the rotating reference frame and interface position between the rotor and stator is updated in each time step. The time step is related to the rotational speed of the rotor. The rotor-stator model is the unsteady solution type of turbomachinery CFD solutions. The main advantage of this model is modeling the transient effects and calculation the losses occurring between the rotating and stationary parts. However the solution periods are longer and more computational power is needed for the solution by means of CPU clock speed and memory of the computer when it is compared to the frozen rotor model. There are studies in the literature where these two models are used simultaneously.

The second important aim of application of CFD analyses to the pumps is improving the pump characteristics by means of hydraulic efficiency. Nevertheless in order to perform full CFD analyses for improving the hydraulic characteristics of the pumps require, selection of proper boundary conditions, generating high quality sets of elements and choosing proper turbulence model. There are several boundary condition definitions applied to the inlet and outlet of the pump. For numerical stability reasons, two additional volumes are added to the inlet and outlet of the pump stage and the boundary conditions are defined at the faces of these volumes. In most of the applications, velocity is specified at the entire inlet face of the inlet domain and pressure rise is specified at the outlet face of the outlet domain. The total number of elements that are generated for the solution domain affects the solution in the pump analyses. The number of elements that is generated by the commercial CFD software is related to the memory capacity of the computer used for analyses. It is possible to find out mesh independency limit of total number of elements in steady state solutions that are applied to the pumps by using frozen rotor model. However in transient analyses that are performed on the pumps do not demonstrate mesh independence solutions due to turbulence models. It is known that in order to find out the suitable number elements that are required to minimize the errors in the calculations that are performed in CFD analyses, the output of the code should be verified with the real life experiment results.

1.5 THESIS STRUCTURE

This chapter consists of the objectives and methodology of the thesis work with a brief introduction of important facts and information related to the subject matter of the thesis.

Chapter 2 summarizes previous work published in different articles and journals related to the thesis. Also, gap in study is dealt briefly.

Chapter 3 introduces CFD concisely with discretization in solving fluid flow also gives the brief details of multiphase flow and demonstrates the numerical approaches for multiphase flow in CFD. The different models for solving multiphase flow are explained. The last part contains the drawbacks found in the existing pump.

Chapter 4 is mainly concentrated upon modifications employed upon the previous design of the pump. Two cases have been taken and a detailed study has been done on them. A final improved design of the pump has been obtained.

Chapter 5 deals with the additional modification possible with the existing design. In this section effect of number of blades has been studied.

Chapter 6 comprises of important conclusions and results obtained during the study of the modifications done on the pump. Future scope of the work has also been discussed.

CHAPTER 2 LITERATURE REVIEW

At the present time, single and multistage centrifugal pumps are widely used in industrial and mining sectors. Centrifugal slurry pumps are meant for handling slurry mixture differ in many aspects as compared to that of conventional pumps used for clear liquids. The performance of the centrifugal slurry pumps is very important in the successful operation of the slurry transportation system. There are many design parameters for pumps, which affects the characteristics of pump immensely. To achieve better performance for a centrifugal pump, design parameters such as the number of blades for impeller-diffuser, blade angle, blade height and diffuser, blade width, impeller diameter, and volute casing radius must be determined accurately, due to the complex liquid flow through a slurry pump. A lot of papers have been published on various aspects of wear in a slurry impeller or volute, performance corrections and derating, etc. The readers of these papers are often left with the impression that the design of these pumps is a combination of science and art. What are generally lacking in the research work are the guidelines for the design of slurry pumps**.** This chapter deals with the literature review of experimental and numerical evaluation of performance characteristics of centrifugal pump.

Benretam et al. (2007) conducted experimentation on the 6 bladed centrifugal pump to investigate the effect of solid particles on centrifugal pump performance. The slurry used in the experimental work was made with wet phosphate having density 2800kg/m^3 and a maximum solid particle diameter of 3 mm. Certain correction factors were provided after the test. They found that the correction factors vary with solid concentration, particle sizes, solid particle shape and mixture density. Also, the mixture concentration had more significant effect on the pump characteristics than any other parameter. The head reduction factor and efficiency were almost similar for concentrations lower than 15%.

Tang et al. (2007) developed a large eddy simulation code using a dynamic second-order sub-grid-scale (SGS) stress model. The developed code was used to model the governing equations of dense turbulent particle-liquid two-phase flows in a rotating coordinate system, in which continuity is conserved by mass-weighted method to solve the filtered governing equations. The SIMPLEC algorithm was used for the solution of the descritized governing equation. Effect of varying particle number was done for a constant velocity of 5 m/sec. They found the computational result to be in good agreement with the experimental one.

Wennberg et al. (2008) predicted the performance of centrifugal pumps handling complex slurries. Various experimental results were discussed and found, to give maximum deratings in head and efficiency of about 10 and 15 %, provided stable head curves can be maintained. They found that magnified shock losses, circulatory flows and blockage of slurry and vapour tendencies in the pump entrance region were the reasons behind unstable head curves together with the flow behaviour of the slurry.

Kumar et al. (2008) carried out the experimental and computation analysis for the pressure drop across a 90^0 horizontal pipe bend in a slurry pipeline conveying silica sand. The experiments were performed at three different efflux volumetric concentrations (0%, 3.94% and 8.82%) of 448.5 µm silica sand particles with varying the velocity from 1.78 to 3.56 m/s. CFD analysis was carried was carried out to evaluate the pressure drop. CFD modeling gave fairly accurate pressure drops (within a percentage error of ± 10%) for the flow with particle diameter 448.5 µm in the volumetric concentration range 0-8.82% at flow velocities in the range 1.78-3.56 m/sec. Further, they found that the pressure at the outer wall was greater than that at the inner wall and velocity and concentration distribution of solids became more uniform in the downstream flow. Also, the pressure, velocity and concentration profiles were not affected along upstream of the pipe bend.

Liu et al. (2009) analyzed the liquid-solid two phase flow in FGD system pump using CFD tool. The effects of the volume fraction solid phase, particle diameter on the external characteristic of pump were obtained. They found that the distribution of the solid particles was very uneven and solid particles clanged in the impeller passage and even stroked the pressure face. Also, the volume fraction of solid phase in pressure phase was higher than that in suction face, which could cause the wear and tear in the outlet of the impeller. They further concluded that the particle size has more effect on the distribution of the particles and the particles with large size tend to pressure face.

Hedi et al. (2010) studied the effect of various volute designs on the performance of centrifugal pump using CFD tool. Viscous Navier-Stokes equations were used to simulate the flow inside the vaneless impeller and volute. The detailed flow structures for different volute tongue geometries were studied in detail. the numerical calculations were compared with experimental data and good agreement was found. Finally, a solution method was developed to obtain three-dimensional velocity and pressure distribution within a centrifugal pump.

Houlin et al. (2010) studied the effect of blade number on the performance of centrifugal slurry pump. Blade number was varied to 4, 6, 7 with the casing and other geometric parameters kept constant. The inner flow fields and characteristics of the centrifugal pumps with different blade number were simulated and predicted in non cavitation and caviation conditions by using commercial code FLUENT. Rapid protoyping method was employed to make impellers with different blade numbers, and characteristics of prototypes were also tested in an open loop. The prediction values were compared with experimental results, and it was found that the prediction results were well satisfied. The maximum discrepancy of prediction results for head, efficiency and NPSH were 4.83%, 3.9% and 0.36 m, respectively. They finally concluded that blade number change had an important effect on the area of low pressure region behind the blade inlet and jet-wake structure in impellers.

Ngoma et al. (2011) numerically investigated the effect of design parameters, such as: blade height, blade number, outlet blade angle, blade width, and impeller diameter, on the steady state liquid flow in a three-dimensional centrifugal pump. Three cases were considered in their study: impeller, impeller-volute combination, and impeller- diffuser combination. Also, continuity and Navier-Stokes equations with the k-ε turbulence model and the standard wall functions were used by means of ANSYS-CFX code. They found that the design parameters considered by them, affects centrifugal pump performance describing the pump head, BHP, and the overall efficiency. To validate their findings, they have compared numerical simulation results with the experimental results considering the case of combined impeller and diffuser.

Rababa et al. (2011) investigated the influence of blade number and impeller shape on inner flow filed and characteristics of centrifugal pump. It consisted of 3 models of impeller with blade number 2, 3 and 4. Two of these models having 3 blades with additional short blades and the third model also having 3 blades but with an increment in blade thickness of outlet part. The geometrical profile of impeller blades was identical with same withdrawal pump (same volute casing). Simulation was carried out for characteristic curves and inner flow field of the centrifugal pump with different blade number and shape. The experiments were carried out at hydraulic laboratory in hydraulic bench test and compared with the simulated result which indicated that predicted result were better. The experiment concluded that the presence of short blades increased the pump head by 4%, with significantly reduced flow areas in the wheel which did not recommend use of such wheel for groundwater pump. For groundwater pump, it was advised to use four-bladed impeller whereas for large inclusion use three and two bladed impeller.

Singh et al. (2011) investigated the effect of geometric parameters of a centrifugal fan with backward- and forward-curved blades. An experimental setup was developed and prototypes of fans were made to carry out measurements of flow and power consumption by the fan. The fan mounting setup was such that fan with uniform blades could be tested. They also developed a patented design of shaft that would enable mounting of fan with uniform blades on the vehicle. A computational fluid dynamics (CFD) model was developed for the fan and the results were validated with the experimental measurement. Further, parametric studies were carried out with number of blades, outlet angle and diameter ratio, to quantify the power coefficient, flow coefficient, efficiency and flow coefficients.

LI et al. (2011) studied the hydraulic performance of a centrifugal pump with a larger exit blade angle numerically with the CFD code Fluent for the pump handling water and different viscous oils. The performance and flow was investigated at an exit angle of 44° and compared with that of a pump with an exit blade angle of 20°. Three fluid domains coexisted in the computational model. Fresh water, oil 1, oil 2 and oil 3 were used as the working liquid. Thirteen working conditions were specified to cover the flow rate range of 1.0 – 11.0L/s for the pump in the numerical computations. They found that the flow in the impeller with a large exit blade angle was subjected to separation near the blade pressure side, however, a large exit blade angle helped to improve the pump performance of viscous oil and increased in the hydraulic loss over the entire flow rate range in the volute. The flow in the impeller with a large exit blade angle acquired a separated structure near the pressure side of the blade even at the point of best efficiency.

Djerroud et al. (2011) performed the numerical investigation of the effects different design parameters, including the blade height, the blade number, the outlet blade angle, the blade width, and the impeller diameter, on the steady state liquid flow in a three-dimensional centrifugal pump. Three cases were considered for the study: impeller, combined impeller and volute, and combined impeller and diffuser. The continuity and Navier-Stokes equations with the k-ε turbulence model and the standard wall functions were used by means of ANSYS-CFX code. The results revealed that the selected key design parameters had an impact on the centrifugal pump performance describing the pump head, the brake horsepower, and the overall efficiency. To validate the developed approach, the results of numerical simulation were compared with the experimental results considering the case of combined impeller and diffuser.

Yang et al. (2011) adopted numerical method to investigate main geometric parameters of pump volute, including volute throat area, volute cross section shape, design rule of spiral development area, and radial gap between impeller and volute tongue to pump performance. A design method of high-efficiency pump volute was developed through the influence of volute main geometric parameters to pump performance.

Singh et al. (2012) studied the characteristics of low specific speed centrifugal water pump. The characteristics were evaluated by studying the relationships among the impeller eye diameter, vane exit angle. They found that the discharge is greatly affected by any resistance to flow, outlet conditions, design parameters of impeller and casing, and width of the blade at exit. Different pump models were developed by varying critical design parameters to different levels. ANSYS-FLUENT code was applied to solve numerically equations and to perform numerical simulations, which were carried out to analyze the effects of the key design parameters, including the eye diameter, the outlet blade angle and the blade width at exit had on the pump performance.

Shojaeefard et al. (2012) studied the effect of change in the outlet angle and passage width of the impeller,. The finite volume method was used for the discretization of the governing equations, and the High Resolution algorithm was employed to solve the equations. The k - epsilon SST model was adopted as the turbulence model in the simulation. They found that increasing the passage width of the impeller passage from 17 to 21 mm increased the head and hydraulic efficiency due to reduction of the friction losses. Also, the centrifugal pump performance with the impeller passage width equal to 21 mm, at outlet blade angle of 30 had better pump performance than with 27.5 mm. and 32.5 mm due to reduction of the dissipation raised by vortex formation in impeller passage when the pump handles viscose liquid.

Wei et al. (2012) conducted numerical simulation on WQS120-60-45 type of sewage pump for the analysis of internal two-phase flow. The distribution of the solid particles in impeller was observed, and the influence of impeller outlet angle on pump efficiency and the ability of solid particles passing through were analyzed. The results showed that the solid particles concentrated on pressure surface of impeller. When impeller outlet angle was higher, local medium energy lost seriously. With the angle decreasing, the blade was more suitable for the flow of the solid particles, which improved the impeller wearing and increased efficiency.

Singh et al. (2012) discussed an application of the Taguchi method for optimizing the design parameters in blower operation. It was found that impeller dimensions were significantly improved the performance of blower by conducting experiments at the optimal parameter combination. The four most influenced identified parameters were (A) Impeller outer diameter; (B) Impeller width; (C) Blade Thickness and (D) Impeller inlet diameter which affect the performance of blower. CFD results were validated by the fine conformity between the CFD results and the experimental results.

Rajendran et al. (2012) used ANSYS software package to develop a three dimensional, fully turbulent model of the compressible flow across impeller of a centrifugal pump. The flow patterns through the pump, performance results, circumferential area averaged pressure from hub to shroud line, blade loading plot at 50 % span, stream wise variation of mass averaged total pressure and static pressure, stream wise variation of area averaged absolute velocity and variation of mass averaged total pressure contours at blade leading edge and trailing edge for designed flow rate are presented.

Grewal et al. (2012) developed a High-velocity Slurry Erosion Test Rig using CFD. They discussed that the newly designed test rig could possibly eliminate some of the limitations (velocity-concentration interdependence and lack of acceleration distance) found in the existed set-ups. Calibration of the test rig was done for jet velocity and erodent concentration. Commissioning of the rig was undertaken by evaluating the effect of operating parameters (concentration and impingement angle) on the erosion rates of aluminum and cast iron. They found that the rig was able to capture the traditional responses of ductile and brittle erosion behaviors of the materials. Repeatability of the test rig was ensured, and the results were found to be within the acceptable error limits.

Han et al. (2012) simulated the solid-liquid two-phase unsteady flow in a screw centrifugal pump with unsteady Reynolds averaged Navier-Stokes equations and sliding mesh technology. The distribution of the pressure at volute outlet, radial force, axial force and total moment were presented. They found that there were lesser effects on the fluctuation trend and direction of the force in pressure at volute outlet, radial force, axial force and total moment, but the values increased with the increasing of solid-volume fraction. The value of total moment on the impeller was minimum when the Rmax just turned tongue of volute. The pressure on the monitoring points had fluctuations with different waveform during one period, it depended on the location of the monitor point and the interaction of impeller and volute. There was little effect of the solid-volume fraction on the pressure fluctuation on the monitor points of the volute and the values of pressure on monitoring points increased with increasing of solid volume fraction. The pressure fluctuation on the monitor points had different trends during one period, which depends on the direction of the monitor points and the rotor-stator interaction strength of impeller and volute.

Kaushal et al. (2012) numerically simulated slurry flow in pipeline of mono-dispersed fine particles at high concentration using Mixture and Eulerian two-phase models. They compared computational data with experimental data collected in 54.9 mm diameter horizontal pipe for concentration profiles at central vertical plane using c-ray densitometer and pressure drop along the pipeline using differential pressure transducers. Experiments were performed on glass beads with mean diameter of 125 lm for flow velocity up to 5 m/s and four overall concentrations up to 50% (namely, 0%, 30%, 40% and 50%) by volume for each velocity. They found that the modeling results by both the models for pressure drop in the flow of water were found to be in good agreement with experimental data. For flow of slurry, Mixture model failed to predict pressure drops correctly. The amount of error increased rapidly with the slurry concentration. Although the Eulerian model gave fairly accurate predictions for both the pressure drop and concentration profiles at all efflux concentrations and flow velocities. Velocity and slip-velocity distributions, that had never been measured experimentally at such higher concentrations, was predicted by Eulerian model.S lip velocity between fluid and solids dragged most of the particles in the central core of pipeline, resulting point of maximum concentration to occur away from the pipe bottom.

Kumar et al. (2012) investigated experimentally the erosive wear on the high chrome cast iron impeller of slurry disposal pump using response surface methodology. They suggested that Erosive wear occurs on the impeller and volute casing of the slurry disposal pump due to the impact of the ash particles on the impeller with a high velocity. Also, due to erosive wear, pump life become very short. The experimental investigation of erosive wear was carried out on the high speed slurry erosion tester to understand the effects of the ash concentration in slurry, rotational speed of the pump impeller and ash particle size on erosive wear. The erosive wear behaviour of high chrome cast iron was investigated by Response surface methodology (RSM). Analysis of variance (ANOVA) was used for statistical analysis and the modeled values for the response were obtained with the help of modeled equation. The found that the ash concentration in slurry and kinetic energy of the moving particles highly contributed to erosive wear of pump impeller as compared to the ash particle size. Also, erosive wear of the pump impeller decreased with decreasing ash concentration, rotation speed and particle size.

Lipsett et al. (2012) considered modeling of wear damage in flotation cells, which were widely used in mineral processing. Empirically developed equations for the flow field of cylindrical mixing vessel with a Rushton turbine were used in formulating a model relating the damage accumulation rate with a simple set of measurable variables. To validate a model, a PIV technique was used to measure velocities in the flow field and near the wall on a physical model of the cell with transparent walls and particles that match the refractive index of the fluid. An Eulerian–Langrangian approach was used to determine the particle trajectories and the effect of a squeeze film was incorporated into the model to modify the velocity distribution of particles prior to impacts. An analytical model based on equations of impulse and momentum for a particle of any shape striking a flat massive surface was used to describe the energy lost at the walls. Finally, a damage model was developed that takes into account impact velocity, attack angle, properties of the impinging particles and the surface. The model was then verified against a second physical model that measures material loss rate at different locations within the cell.

Liu et al. (2012) studied the pattern of solid-liquid two-phase distribution in chemical process pump. In order to explore the pattern of solid-liquid two-phase flow distribution in first stage of double-suction impeller and the double volute channel of the HD type petrol-chemical process pump, the flow field in double-suction impeller and double volute was simulated with the CFD software. The Reynolds Averaged Navier Stokes equations were taken as the governing equations, and the standard k-εmodel for turbulence. The pattern of solid particle concentration distribution in the impeller and double volute channel under different initial particle concentrations and different particle diameters were derived. They found that in the double-suction impeller, solid phase distribution changed a lot along with the increase of initial particle concentration; the concentration near the back side was higher than the face side. Solid particles had the motion trend to the back side of blade in double-suction impeller along with the increased particle diameters. In double volute channel, solid phase concentration distribution was uneven and solid particle concentration was relatively higher from section 1 to section 8. In the diffusion section, concentration was high in lateral side and low in medial side, also, the solid particles had the motion trend to the lateral side and the solid particle concentration was relatively higher.

Yi et al. (2012) performed the numerical simulation and experimental research on the influence of solid-phase characteristics on centrifugal pump performance. Two-phase numerical simulation and centrifugal pump performance tests were carried out using different solid particle diameters and two phase mixture concentration conditions. It was difficult to examine the solid-liquid two-phase turbulent flow in the pump as the law governing the movement of particles in the centrifugal pump channel was very complicated. Consequently, the solid-liquid two-phase pump was designed based only on the unary theory. They found that the obvious variety of centrifugal pump internal flow appeared because of the existence of solid phase and hence, pump performance was changed. Inner flow features were revealed by comparing the simulated and experimental results. After the results were compared it was found that the influence of the solid phase characteristics on centrifugal pump performance was smaller when the flow rate was low, specifically when it was lesser than 2 m^3/h. The maximum efficiency declined, and the best efficiency point shifted along the low flow rate direction along with increased solid particle diameter and volume fraction. The variation in the tendency of the pump head was basically consistent with the efficiency. The efficiency and head values of the two phase mixture transportation were even larger than those of pure water transportation under smaller particle diameter and volume fraction conditions at the low flow rate region. They further concluded that change of the particle volume fraction had greater effect on the pump performance than the change in the particle diameter. And, the experimental values were smaller than the simulated values.

Zhao et al. (2012) performed the numerical investigation of solid-liquid two phase flow in a non-clogging centrifugal pump at off-design conditions. The solid-liquid two-phase flow fields in the non-clogging centrifugal pump with a double-channel impeller were investigated numerically for the design condition and also off-design conditions, in order to study the solid-liquid two-phase flow pattern and non-clogging mechanism in non-clogging centrifugal pumps. They found that the sand volume fraction distribution was extremely inhomogeneous in the whole flow channel of the pump at off-design conditions and in the impeller; particles were mainly flowing along the pressure surface and hub. In the volute, particles mainly accumulated in the region near to the exit of volute, the largest sand volume fraction was observed at the tongue, and a large number of particles collide with volute wall and exit the volute after circling around the volute for several times. When the particle diameter was increased, particles accumulated on the pressure side of the impeller, and more particles crashed with the pressure side of the blade. Larger sand volume fraction gratitude was also observed in the whole flow channel of the pump. Also, with the decrease of the inlet sand volume fraction, particles accumulated on the suction side of the blade. They further concluded that compared with the particle diameter, the inlet sand volume fraction had less influenced the sand volume fraction gratitude in the whole channel of the pump. Also, at the large flow rate, the minimum and maximum sand volume fraction in the whole flow channel of the model pump was smaller than that at the small flow rate and the water transportation capacity increased with the flow rate.

Zhang et al. (2013) has numerically simulated and analyzed the solid-liquid two-phase flow in centrifugal pump. He has done a 3D, steady, incompressible, and turbulent solid-liquid two-phase flow analysis in a low specific speed centrifugal pump. He used the CFD code based on the mixture model and the RNG *k*-e two equation turbulence model for two phase flow analysis, in which the influences of rotation and curvature were taken into account. He used the frozen rotor method to define coupling between impeller and volute of the pump. He found that the solid phase properties in two-phase flow, especially concentration, particle diameter and density, have strong effects on the hydraulic performance of the pump. He also observed that pump head and efficiency are reduced with increasing particle diameter or concentration. However, he also suggested that the effect of particle density on the performance of the pump is relatively lower. He observed an obvious jet-wake flow structure near the volute tongue and which became more remarkable with increasing solid phase concentration. Further, he found that suction side of the blades as more prone to abrasion than the pressure side.

CHAPTER 3 COMPUTATIONAL FLUID DYNAMICS AND SCOPE OF IMPROVEMENT

3.1 COMPUTATIONAL FLUID DYNAMICS

CFD is the science in which different phenomenons occurring in a real life system or process such as: flow, heat transfer, mass transfer, chemical reactions etc., are studied/predicted by solving the mathematical model based numerical methods and algorithms. There are many commercial CFD packages like FLUENT, ICEM-CFD, STAR CCM+ etc. which consists of user interfaces so that user can get easy access and problem in hand can be modeled with minimum difficulty in the computational environment. High quality computer processors are used to perform the millions of calculations required to simulate the interaction of fluids and gases with the complex surfaces used in engineering. Even with simplified equations and high-speed supercomputers, only approximate solutions can be achieved in many cases. Ongoing research, however, may generate software that can improve the accuracy of the results and speed of complex simulation. The most important consideration in CFD is how the practical system is designed or discretized in the computational environment. One method is to discretize whole system domains into small cells to form a grid, and then apply a suitable algorithm to solve the equations of motion (Euler equations for inviscid and Navier-Stokes equations for viscous flow) on every cell. These small cells or mesh can either be irregular (different design: triangular in 2D or pyramidal in 3D cases) or regular; the distinguishing characteristic of the former is that each cell must be stored separately in memory. Where shocks or discontinuities are present, high resolution schemes such as Total Variation Diminishing (TVD), Flux Corrected Transport (FCT), Essentially Non Oscillatory (ENO), or MUSCL schemes are needed to avoid spurious oscillations (Gibbs phenomenon) in the solution. If one chooses not to proceed with a mesh-based method, a number of alternatives exist, notably Smoothed particle hydrodynamics (SPH), a Lagrangian method of solving fluid problems, Spectral methods, a technique where the equations are projected onto basis functions like the spherical harmonics and Chebyshev polynomials, Lattice Boltzmann methods (LBM), which simulate an equivalent mesoscopic system on a Cartesian grid, instead of solving the macroscopic system (or the real microscopic physics). It is possible to directly solve the Navier- Stokes equations for laminar flows and for turbulent flows when all of the relevant length scales can be resolved by the grid (a direct numerical simulation). In general however, the range of length scales appropriate to the problem is larger than even today's massively parallel computers can model. In these cases, turbulent flow simulations require the introduction of a turbulence model. Large eddy simulations (LES) and the Reynolds-averaged Navier-Stokes equations (RANS) formulation, with the k-ε model or the Reynolds stress model, are two techniques for dealing with these scales. In many instances, other equations are solved simultaneously with the Navier-Stokes equations. These other equations can include those describing species concentration (mass transfer), chemical reactions, heat transfer, etc. More advanced codes allow the simulation of more complex cases involving multi-phase flows (e.g. liquid/gas, solid/gas, liquid/solid), non-Newtonian fluids (such as blood), or chemically reacting flows (such as combustion).

3.2 DISCRETIZATION METHODS IN CFD

The stability of the chosen discretization is generally established numerically rather than analytically as with simple linear problems. Special care must also be taken to ensure that the discretization handles discontinuous solutions gracefully. The Euler equations and Navier-Stokes equations both admit shocks, and contact surfaces.

Some of the discretization methods being used are:

• **Finite difference method.** This method has historical importance and is simple to program. It is currently only used in few specialized codes. Modern finite difference codes make use of an embedded boundary for handling complex geometries making these codes highly efficient and accurate. Other ways to handle geometries are using overlapping-grids, where the solution is interpolated across each grid.

• **Finite volume method (FVM).** This is the "classical" or standard approach used most often in commercial software and research codes. The governing equations are solved on discrete control volumes. FVM recasts the PDE's (Partial Differential Equations) of the N-S equation in the conservative form and then discretize this equation. This guarantees the conservation of fluxes through a particular control volume. Though the overall solution will be conservative in nature there is no guarantee that it is the actual solution. Moreover this method is sensitive to distorted elements which can prevent convergence if such elements are in critical flow regions. This integration approach yields a method that is inherently conservative (i.e. quantities such as density remain physically meaningful

• **Finite element method (FEM).** This method is popular for structural analysis of solids, but is also applicable to fluids. The FEM formulation requires, however, special care to ensure a conservative solution. The FEM formulation has been adapted for use with the Navier-Stokes equations. Although in FEM conservation has to be taken care of, it is much more stable than the FVM approach. Subsequently it is the new direction in which CFD is moving. Generally stability/robustness of the solution is better in FEM though for some cases it might take more memory than FVM methods.

3.3 CFD METHODOLOGY

Working in CFD is done by writing down the CFD codes. CFD codes are structured around the numerical algorithms that can tackle fluid problems. In order to provide easy access to their solving power all commercial CFD packages include sophisticated user interfaces and input to examine the results.

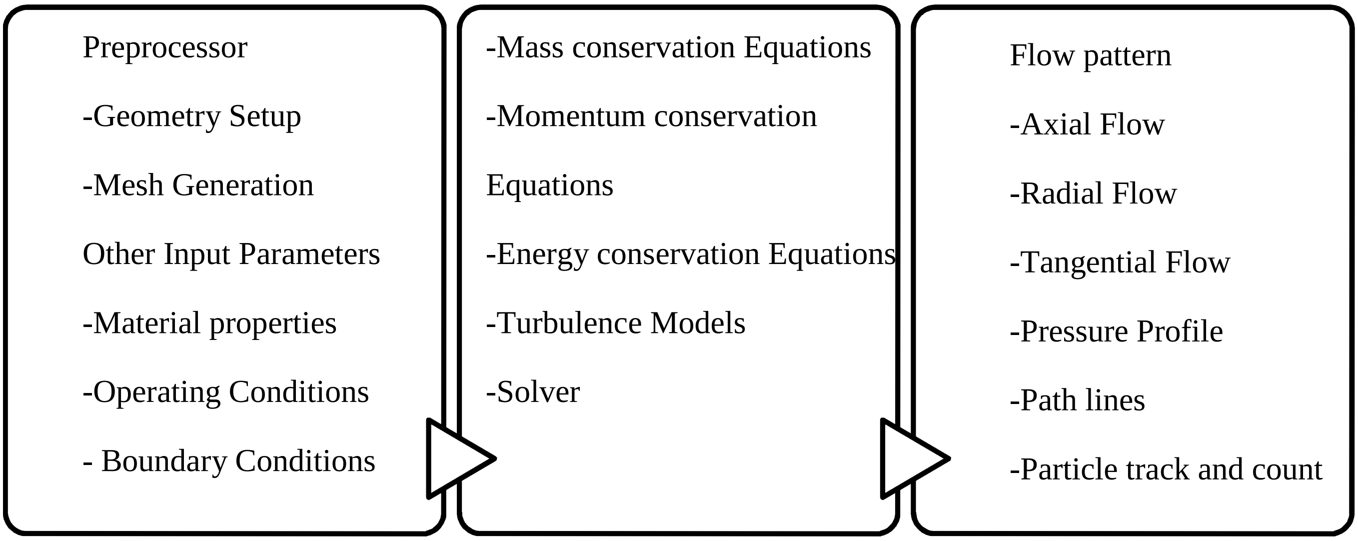

Figure 3.1: CFD processing

Hence all codes contain three main elements:

1. Pre-processing.
2. Solver
3. Post - processing.

Initial design

The first step in CFD processing is constructing an initial design of the system. Initial design can be made directly by measuring the dimensions of the practical system. But in case if a new design has to be proposed then the design must be made by consulting several aspects like: system requirements, load analysis, failure analysis, material characteristics etc.

Geometry generation

Geometry generation can be termed as the most important step in the numerical modelling and simulation because if the geometry generation is not accurate than results can never be close to the practical results no matter how accurate is the definition of the boundary conditions. After the initial design is received it has to be transformed in a computer design or domain. Many commercial modelling softwares are available to model geometry from initial design.

Mesh generation

Meshing or Gridding is the process of subdividing the geometry into a set of small control volumes. With each control volume there will be one or more values of the dependent flow variables (e.g., velocity, pressure, temperature, etc.) associated. Generally, these dependent variables represent certain type of locally averaged values. Numerical algorithms based on conservation laws of mass, momentum and energy are then used to calculate these variables for each control volume.

In general, a mesh network is made up of the geometric arrangement of elements and nodes. Nodes represent points at which certain features such as displacements are calculated. The boundaries of elements are limited by the nodes. Elements define localized mass and stiffness properties of the model. Elements can also be defined by mesh numbers. The mesh numbers allow references for corresponding deflections, stresses, pressures, temperatures at specific locations of the model. The traditional method used for mesh generation is block-structure (multi-block) mesh generation. The block-structure approach is one of the simplest and efficient techniques of mesh generation.

Pre-processing

Pre-processing consists of the input of a flow problem to a CFD program by means of an user-friendly interface and the subsequent transformation of this input into a form suitable for use by the solver. The region of fluid to be analyzed is called the computational domain and it is made up of a number of discrete elements called the mesh (or grid). The users need to define the properties of fluid acting on the domain before the analysis has begun; these include external constraints or boundary conditions, like pressure and velocity to implement realistic situations.

Solver

Solver can be defined as a program that calculates the solution of the CFD problems. Here the governing partial differential equations are solved. A number of iterations are generally done by a solver to compute the flow parameters of the fluid as time elapses. Convergence of the result is very important to produce an accurate solution of the partial differential equations.

Post-processor

Post-processor used to visualize the results obtained from the solver. In a general CFD package, the analyzed flow phenomena can be presented in vector plots or contour plots to display the trends of velocity, pressure, kinetic energy and other properties of the flow.

3.4 NUMERICAL CALCULATION OF MULTIPHASE FLOW

Multiphase systems are very complicated because it contains various phases and each one of these phases affects the behaviour of the system. The multiphase flow system comprises various single phase domains which are covered by moving interfaces. The boundary condition in multiphase system is shared by each single phases. The multiphase system can be designed in terms of certain local variables which is included with all the individual phases. Multiphase systems are very difficult to model and solve. In other words it is almost next to impossible to solve multiphase system directly.

The averaging approach in multiphase flow can be divided in 3 categories, Lagrangian approach, Boltzmann approach and Eulerian approach. These approaches can be further divided in different subgroups based upon different constraints with which the mathematical operator is declared. The two main numerical averaging approach for numerical solution of multiphase flow are explained below:

3.4.1 Eulerian – Lagrangian Approach

The Eulerian-Lagrangian approach is used to model continuous-dispersed systems and is generally called particle transport model. Here, in this approach primary phase is always continuous and is generally composed of fluids (liquid and gas) whereas the secondary phase is droplets, particles or bubbles. In the Eulerian- Lagrangian approach, the primary phase, which the continuum, is used in an Eulerian structure. Navier-Stokes equations are solved in order to compute the primary phase. Foe the dispersed phase a small number of particle stream is taken which represents the whole particle flow and then state and location of each particle stream is computed by solving ordinary differential equation for mass, momentum and energy transfer. Finally, the coupling of two phases is obtained by using appropriate interaction models. This approach is only limited to low-volume fraction flows as volume displaced by the secondary phase is not accounted in this approach.

In this approach the volume displaced by the dispersed phase is not taken into account. So, this approach is applicable for low-volume fractions of the dispersed phase. This approach is applicable for situations in which the discrete phase is injected as a continuous stream into the continuous phase. A force balance equation based on Newton's second law of motion is solved to compute the trajectory of the discrete phase.

The Eulerian-Lagrangian approach is suitable to unit operations in which the volume fraction of the dispersed phase is small, such in spray dryers, coal and liquid fuel combustion, and some particle-laden flow. This approach provides complete information on the behavior and residence time of individual particles. Interaction of individual particle streams with turbulent eddied and solid surfaces such as walls can be modeled.

3.4.2 Eulerian – Eulerian Approach

Eulerian-Eulerian approach is the most general approach for solving multiphase flows. It is based on the principle of interpenetrating continua, where each phase is governed by the Navier-Stokes equations. The phases share the same volume and penetrate each other in space and exchange mass, momentum and energy. Each phase is described by its physical properties and its own velocity, pressure, concentration and temperature field. The interphase transfer between phases is computed using empirical closure relations. The Eulerian-Eulerian approach is applicable for continuous-dispersed and continuous-continuous systems.

For continuous-dispersed systems, the velocity of each phase is computed using the Navier-Stokes equations. The dispersed phase can be in the form of particles, drops or bubbles. The forces acting on the dispersed phase are modeled using empirical correlations and are included as part of the interphase transfer terms. In addition, drag, lift, gravity, buoyancy and virtual-mass effects are some of the forces that might be acting on the dispersed phase. These forces are computed for an individual particle and then scaled by the local volume fraction to account for multiple particles.

There are three different Euler-Euler multiphase models available:

- Volume of fluid method (VOF)
- Mixture model
- Eulerian model

Volume of Fluid Method

In computational fluid dynamics, the Volume of fluid method is one of the most well known methods for volume tracking and locating the free surface. The motion of all phases is modelled by solving a single set of transport equations with appropriate jump boundary conditions at the interface. It can model two or more immiscible fluids by solving a single set of momentum equations and tracking the volume fraction of each of the fluids throughout the domain. Typical applications include the motion of large bubbles in a liquid, the motion of liquid after a dam break, the prediction of jet breakup, and the steady or transient tracking of any liquid-gas interface.

Eulerian Model

Eulerian model is the most general model for solving multiphase flows. The Eulerian model is the most complex of the multiphase models. It solves a set of n momentum and continuity equations for each phase. In the next section, there are more details about Eulerian model.

Mixture Model

The mixture model is a simplified multiphase model that can be used in different ways. The mixture model can apply to model multiphase flows where the different phases move at different velocities and also it is applicable to model homogeneous multiphase flow and to calculate non-Newtonian viscosity. We have used the mixture model to simulate the multiphase flow in our work.

The mixture model can model n phases (fluid or particulate) by solving both the continuity equation and the momentum equation for the mixture, where mixture can be a combination of continuous phase and the dispersed phase. In addition, the mixture model solves the energy equation for the mixture and the volume fraction equation for the secondary phases, as well as algebraic expressions for the relative velocities (if the phases are moving at different velocities). Also it allows us to select the granular phases and we can calculate the different properties for granular phases. It is applicable in the particle-laden flows with low loading, and bubbly flows where the gas volume fraction remains low, cyclone separators, sedimentation and in liquid-solid flows.

Continuity equation for the mixture

First of all, we can write the continuity equation as follow:

$$\frac{\partial}{\partial t}(\alpha_k \rho_k) + \nabla.(\alpha_k \rho_k \vec{v}_k) = \Gamma_k \tag{1}$$

where, α_k is the volume fraction of the kth phase and the term Γ_k represents the rate of mass generation of phase k at interface. From the above equation (1), we obtain by summing over all phases,

$$\frac{\partial}{\partial t}\sum_{k=1}^{n}(\alpha_k \rho_k) + \nabla.\sum_{k=1}^{n}(\alpha_k \rho_k \vec{v}_k) = \sum_{k=1}^{n}\Gamma_k \tag{2}$$

Because of the mass conservation the right hand side of the equation (20) must be vanish, so

$$\sum_{k=1}^{n} \Gamma_k \tag{3}$$

From it, we obtain a continuity equation of the mixture as

$$\frac{\partial \rho_m}{\partial t}(\alpha_k \rho_k) + \nabla.(\rho_m \vec{v}_m) \tag{4}$$

Here the mixture density and the mixture velocity are defined as,

$$\rho_m = \sum_{k=1}^{n} (\alpha_k \rho_k) \tag{5}$$

$$\vec{v}_m = \frac{1}{\rho_m} \sum_{k=1}^{n} (\alpha_k \rho_k \vec{v}_k) \tag{6}$$

The mixture velocity $\vec{v}_m$ represents the velocity of the mass centre. Also ρ_m varies although the component densities are constants. The mass fraction of phase *k* is defines as

$$c_k = \frac{\alpha_k \rho_k}{\rho_m} \tag{7}$$

Equation (4) has the same form as the continuity equation for the single phase flow.

Momentum equation for the mixture

The momentum equation for k^{th} is written as,

$$\frac{\partial}{\partial t}(\alpha_k \rho_k \vec{v}_k) + \nabla.(\alpha_k \rho_k \vec{v}_k \vec{v}_k) = -\alpha_k \nabla \mathrm{p_k} + \nabla.[\alpha_k(\tau_k + \tau_{Tk})] + \alpha_k \rho_k g + M_k \tag{8}$$

where M_k is the average interfacial momentum source for the phase k. τ_k is the average viscous stress tensor and τ_{Tk} is the turbulent stress tensor.

Now the momentum equation for the mixture follows (8) by summing over the phases

$$\frac{\partial}{\partial t}\sum_{k=1}^{n}(\alpha_k \rho_k \vec{v}_k) + \nabla.\sum_{k=1}^{n}(\alpha_k \rho_k \vec{v}_k \vec{v}_k) = -\sum_{k=1}^{n}(\alpha_k \nabla p_k) + \nabla.\sum_{k=1}^{n} \alpha_k(\tau_k + \tau_{Tk}) + \sum_{k=1}^{n} \alpha_k \rho_k g + \sum_{k=1}^{n} M_k \tag{9}$$

By using the definitions (5) and (6) of the mixture density ρ_m and the mixture velocity and the mixture velocity $\vec{v}_m$, the second term of equation (9) can be written as

$$\nabla.\sum_{k=1}^{n}\alpha_k\rho_k\vec{v}_k\vec{v}_k = \nabla.(\rho_m\vec{v}_m\vec{v}_m) + \nabla.\sum_{k=1}^{n}\alpha_k\rho_k\vec{v}_{Mk}\vec{v}_{Mk} \quad (10)$$

Where $\vec{v}_{Mk}$ is the diffusion velocity, i.e., the velocity of the kth phase relative to the centre of the mixture mass

$$\vec{v}_{Mk} = \vec{v}_k + \vec{v}_m \quad (11)$$

The momentum equation takes the form in terms of the mixture variables as,

$$\frac{\partial}{\partial t}(\alpha_m\vec{v}_m) + \nabla.(\rho_m\vec{v}_m\vec{v}_m) = -\nabla \mathrm{p_m} + \nabla.(\tau_m + \tau_{Tm}) + \nabla.\tau_{Dm} + \rho_m g + M_m \quad (12)$$

Where,τ_m, τ_{Tm} and τ_{Dm} are the stress tensors.

Volume fraction equation for the secondary phases

We can obtain the volume fraction equation for secondary phase *p* from the continuity equation of the secondary phase *p* as follow:

$$\frac{\partial}{\partial t}(\alpha_p\rho_p) + \nabla.\alpha_p\rho_p\vec{v}_m = -\nabla.\alpha_p\rho_p\vec{v}_{dr,p} + \sum_{q=1}^{n}(\dot{m}_{qp} - \dot{m}_{pq}) \quad (13)$$

In the mixture model some terms as relative (slip) velocity and drift velocity, interfacial area concentration, solid pressure and granular properties like collisional viscosity, kinetic viscosity, granular temperature are also important.

3.5 TURBULENCE MODELS

Turbulence consists of fluctuations and randomness in the flow field with time and space. It is a complex process, mainly because it is 3D, unsteady and consists of many levels. It affects the flow heavily flow. Turbulence generally occurs when the inertia forces in the fluid become significant compared to viscous forces, and is characterized by a high Reynolds Number. In principle, the Navier-Stokes equations describe both laminar and turbulent flows without the need for additional information. However, turbulent flows at realistic Reynolds numbers span a large range of turbulent length and time scales, and would generally involve length scales much smaller than the smallest finite volume mesh, which can be practically used in a numerical analysis. Turbulence models are used to predict the effects of turbulence in fluid flow without resolving all scales of the smallest turbulent fluctuations. Many models have been developed that can be used to approximate turbulence based on the Reynolds Averaged Navier-Stokes (RANS) equations. Some have very specific applications, while others can be applied to a wider class of flows with a reasonable degree of confidence. One of the main problems in turbulence modeling is the accurate prediction of flow separation from a smooth surface. Standard two-equation turbulence models often fail to predict the onset and the amount of flow separation under adverse pressure gradient conditions. In general, turbulence models based on the two-equations predict the onset of separation too late and under-predict the amount of separation later on. This is problematic, as this behavior gives an overly optimistic performance characteristic of the system. However, we generally use two equation models because of their simplicity and lesser computational time.

K-ε Turbulence Model

One of the most prominent turbulence models, the k -ε (k-epsilon) model, has been implemented in most general purpose CFD codes and is considered as the industry standard model. It has proven to be stable and numerically robust and has a well established regime of predictive capability. For general purpose simulations, the model offers a good compromise in terms of accuracy and robustness. Within FLUENT, the k - ε turbulence model uses the scalable wall-function approach to improve robustness and accuracy near-wall meshes. The scalable wall functions allow arbitrarily solution on finer wall grids, which is a significant improvement over standard wall functions. k - ε turbulence model provide good predictions for many flows of engineering interest. Here, k is the turbulence kinetic energy and is defined as the variance of the fluctuations in velocity. It has dimensions of (L^2T^{-2}) m^2/s^2. ε is the turbulence eddy dissipation (the rate at which the velocity fluctuations dissipate).

K-ω Turbulence Model

One of the advantages of the k - ω formulation is the near wall treatment for low-Reynolds number computations. The model does not involve the complex non-linear damping functions required for other models and is therefore more accurate and more robust. The model assumes that the turbulence viscosity is linked to the turbulence kinetic energy and turbulent frequency via the relation:

$$\mu_t = \frac{k}{\boldsymbol{\omega}} \tag{14}$$

μ_t= turbulence viscosity

k is turbulence kinetic energy and is defined as the variance of the fluctuations in velocity

ω = turbulence frequency

Shear-Stress-Transport Model

The Shear-Stress-Transport model was designed to give highly accurate predictions of the onset and the amount of flow separation under adverse pressure gradients by the inclusion of transport effects into the formulation of the eddy-viscosity. This results in a major improvement in terms of flow separation predictions. The SST model is recommended for high accuracy boundary layer simulations.

3.6 PERFORMANCE CHARACTERISTICS OF PUMP

In following equations are solved for incompressible fluid flow:

A. Continuity Equation

$$\rho(\nabla\vec{v}) = 0 \tag{15}$$

ρ is the density.

$\vec{v}$ is the absolute velocity.

B. Momentum conservation equation

$$\nabla.(\nabla\vec{v}\vec{v}) = -\nabla p + \nabla.(\bar{\bar{\tau}}) + \rho\vec{g} + \vec{F} \tag{16}$$

$\bar{\bar{\tau}}$ is the stress tensor

$\vec{g}$ is the acceleration due to gravity

$\vec{F}$ is the force

p is the pressure

C. Energy Conservation Equation

$$\frac{\partial}{\partial t}(\rho_i) + \nabla.(\rho_i v) = -p\nabla.v + \nabla.(k\nabla \mathrm{T}) + \varphi + \mathrm{S_i} \tag{17}$$

ρ – is the density of fluid

k- thermal conductivity

φ- dissipation

S_i-heat generation

p- is the pressure

T is the terminal Energy per unit volume

Following equation can be used to calculate the Head and Power output of the pump using simulation result:

A. Calculation of Head (H_{Total}):

$$H = (\frac{P_d}{\rho g} + Z_d) - (-\frac{p_s}{\rho g} - Z_s) + \frac{V_d^2}{2g} - \frac{V_s^2}{2g} \tag{18}$$

Where,

V_d = velocity of fluid in delivery pipe (m/s)

V_s = velocity of fluid in suction pipe (m/s)

Z_d = delivery head (meters)

Z_s = Suction lift (meters)

$(\frac{P_d}{\rho g})$ = Delivery pressure gauge reading delivery side (m)

$(\frac{P_s}{\rho g})$ = Vacuum gauge reading at suction side (m)

B. Power output:

$$P_{out} = \rho g Q H \tag{19}$$

Where

H =Total head (m)

ρ = mass density of water, kg/m^3

g = gravitational acceleration m/sec^2

Q = flow rate, m^3/s

P_{out} = Output power, kW

3.7 MODELING AND SIMULATION USING CFD

We have used the modeling software GAMBIT 2.3.16 for making the geometry of the existing model (with blade number 5) and other models of centrifugal slurry pump. FLUENT 6.3.26 simulation software has been used for single phase and multiphase analysis. Fluent tutorial guide has been followed to carry out simulation setting for the analysis of models. The geometrical specification of the existing model of the pump has been given in the table 3.1.

Modeling in Gambit

The existing centrifugal pump contains following three parts.

1. Impeller
2. Casing
3. Inlet passage

Table 3.1: Specification of existing centrifugal slurry pump

Specification	
(a) Impeller	
Type	Closed
Material	Ni-hard
Number of blade	5
Impeller eye diameter(mm)	110
Impeller outlet diameter(mm)	265
Impeller width at eye(mm)	44.2
Impeller inlet vane angle(degree)	23
Impeller outlet vane angle(degree)	25
Impeller width at outlet(mm)	68.59
(b) Casing	
Type	Single volute
Material	Ni-hard
Base volute diameter (mm)	275
Volute width(mm)	85
(c) Inlet passage diameter(mm)	100
(d) Out let passage diameter(mm)	50
(e) Operating speed(rpm)	1450
Non-dimensional Specific speed	0.06957
Minimum Rated speed (rpm)	1450
Best efficiency point head (mwc)	15.1
Rated discharge (lps)	15.1
Maximum efficiency (%)	46%
Pump input power (kW)	4.86

The modeling of the Existing Pump was already done in earlier work [22]. And the geometry of other models has been done by taking the dimensions of the Existing pump as reference. Figure 3.2 shows the geometry created using GAMBIT software.

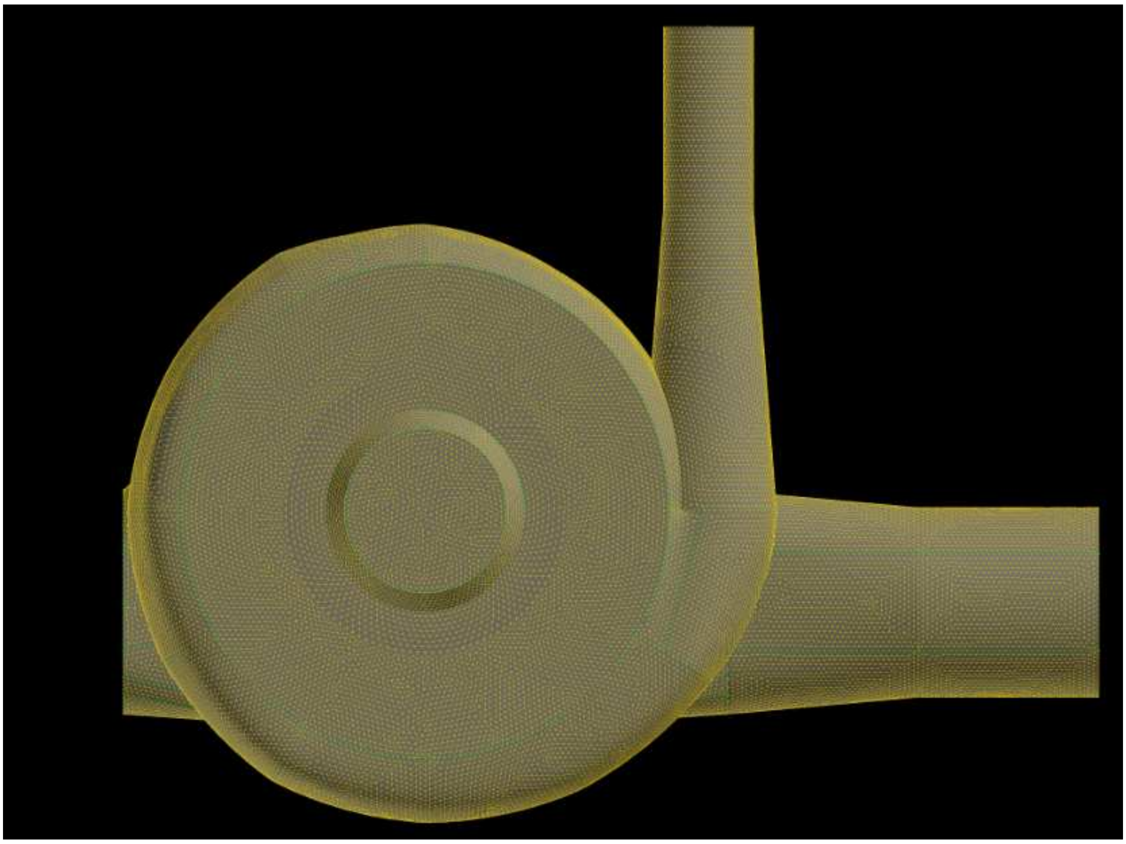

Figure 3.2: Existing centrifugal slurry pump

Meshing

A tetrahedral-hex core meshing is done for all the models of the centrifugal slurry pump. Fine meshing is done for the regions were the forces are more significant and coarser meshing size function is used for all other regions. Grid sensitivity tests have also been done for all the models. As far as the analysis of the pump is concerned a finer meshing scheme is used to take in consideration of the every vital fact which is affecting the flow in case of single as well as multi-phase flow.

Boundary Conditions

Figure 3.4 shows the boundary conditions applied at different surfaces for all the models. A velocity inlet boundary condition is applied at the inlet of the pump. Gauge pressure selected is 101325 Pascal. An outflow boundary condition is selected for the outlet of the pump with flow rate weighting =1. Rest of the sections of the slurry pump is taken as walls. A no slip boundary condition is taken for the wall boundaries where the velocity of the stream increases from zero to the free stream velocity accordingly from the wall. The effect of gravity is also considered in negative Y-axis direction.

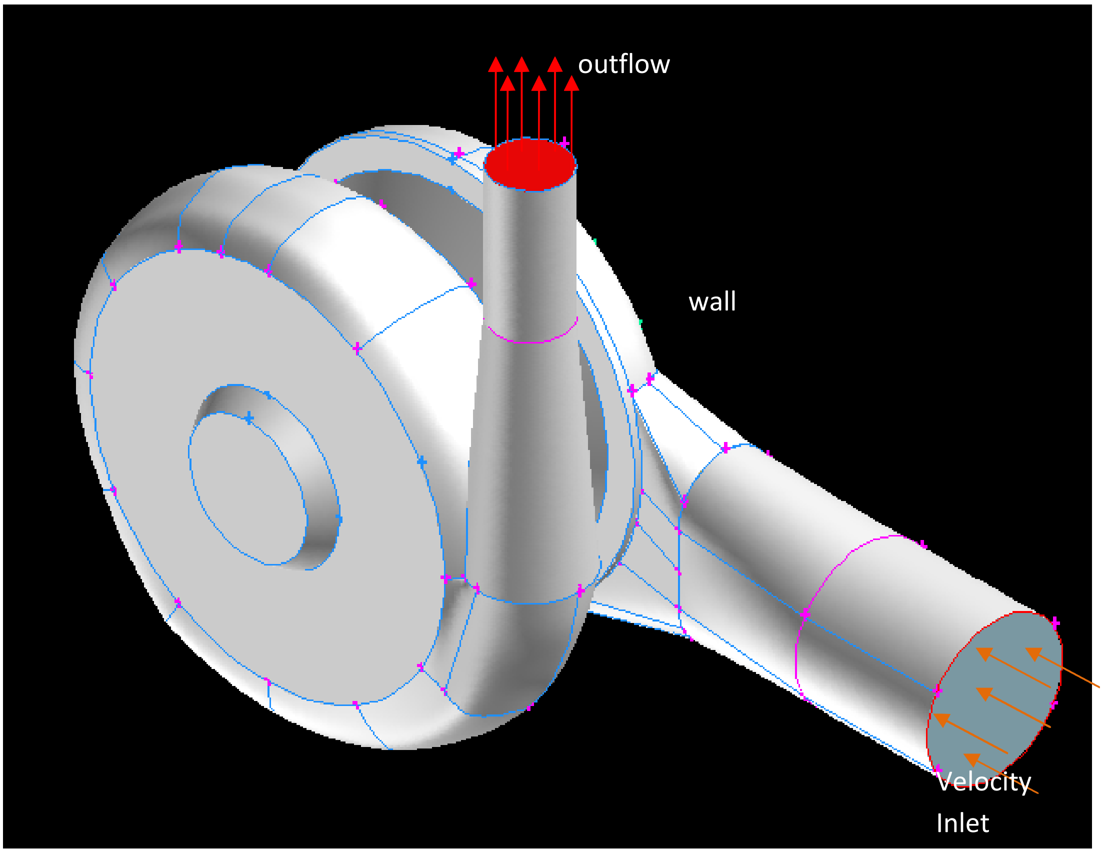

Figure 3.3: Boundary conditions at different surfaces

3.8 IMPORTANT OBSERVATIONS AND DRAWBACK IN EXISTING DESIGN

In this section, important contours [22] for the existing design of pump are analyzed for finding the drawbacks in design of the pump. These drawbacks have been taken in consideration for making design modifications to the Existing Pump. Although the pump is working well near the BEP, but there are certain drawbacks seen, when pump is operating at off-design conditions:

3.8.1 Cutwater Region

When a centrifugal slurry pump is operated at partial capacities beyond BEP it is unable to bear the load of the system for which the hydraulic losses would be minimum. The system attempts to meet the designated flow rate against a system which cannot afford it, so an appreciable amount of flow is recirculated back towards the volute region across the cutwater zone. It results in a high velocity component bound towards the belly region of the centrifugal pump. This recirculted flow component must be guided very well as the cutwater portion is abraded due to impact friction employed by the flow over cutwater region. Following is the diagram for the flow inside the pump at cutwater region for (Q/Q_{BEP}=0.2).

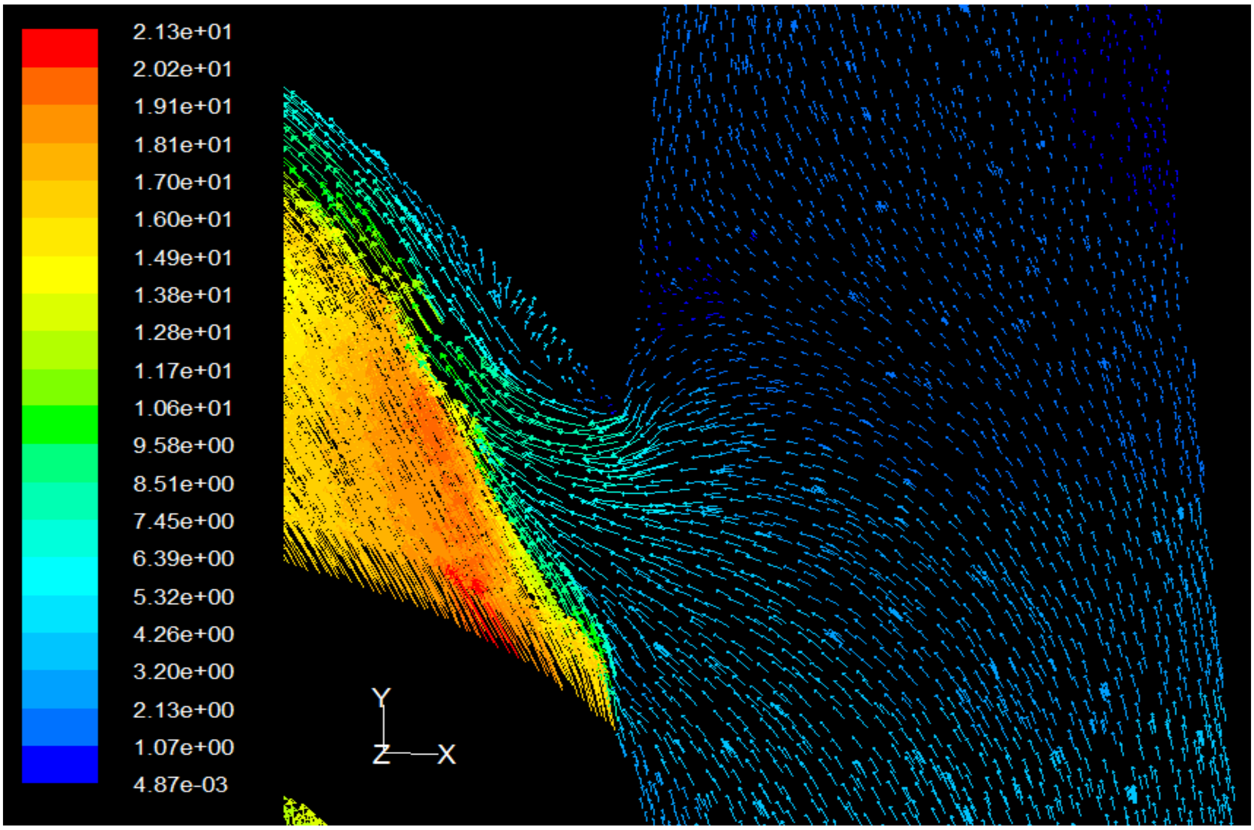

Figure 3.4: Velocity Vector contour for water at 1450 rpm and (Q/Q_{BEP}=0.2) near Cut water region

3.8.2 Tongue region

Following are the contours of static pressure at the mid span for the 20% and 50% (by weight) at 13.12 kg/s mass flow rate and 1450 rpm (BEP):

Figure 3.5: Static Pressure contour for concentration of Bottom Ash (20% by weight) at 1450 rpm and (Q/Q_{BEP}=1)

Figure 3.6: Static Pressure contour for concentration of Bottom Ash (50% by weight) at 1450 rpm and (Q/Q_{BEP}=1)

From the above pressure contours it is but obvious that the pressure increases gradually along the stream wise direction inside the impeller blade passage. But, the pressure stream lines are not perpendicular to the blade passage wall inside the passageway. It is evident that the pressure at the suction side for the same impeller radius is lower than the pressure on the pressure side. Also the pressure is lowest just after the leading edge of the impeller blade passage at the suction side. Further, at the tongue outlet there is always a low pressure region and it is also evident that the span of this low pressure region increases with the increase in the concentration of the bottom ash as in above case the low pressure span at the outlet is greater for the 50% concentration. So, it can be concluded that there is a scope to improve the near tongue region of the pump.

CHAPTER 4 MODIFICATION IN EXISTING CENTRIFUGAL SLURRY PUMP

In the present chapter we have given certain design improvement suggestions after analyzing the previous work [22] with existing design centrifugal slurry pump having blade number 5. In order to make design improvements first of all the results and contours of previous computational analysis is thoroughly studied and then new designs were suggested with the existing pump (blade number 5). The noticeable drawbacks in design have been discussed in previous chapter. Although there were a very little drawbacks with the existing pump at B.E.P but at off design conditions, significant improvements are obtained after employing the modifications in design. For the analysis and study of the new models we have taken the single phase flow module in which water is the working fluid.

4.1 MODIFICATION IN DESIGN

Considering the drawbacks in existing design we have made two cases, first design modification has been employed to the tongue region of the pump and second one is employed with the cutwater area of the volute casing.

4.1.1 CASE I: Effect of Discharge Slope

In the first case we have taken the effect of discharge slope of the slurry pump. For this we have taken 3 models: existing model, straight discharge model and slanted discharge model. Several other researchers like Pagalthivarthi et al. (2011), also considered the effect of discharge slope on abrasive characteristics of flow inside a slurry pump. We have taken the effect of discharge slope to obtain the variation in Head of the slurry pump. Figure 4.1 shows the design of volute casing tongue for the three models. The existing model has a converging discharge slope. The results from

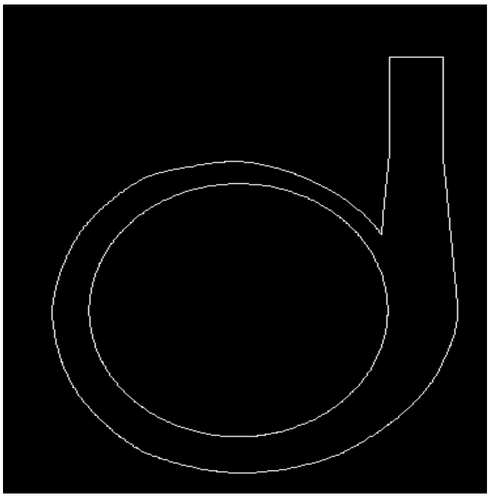

(a)

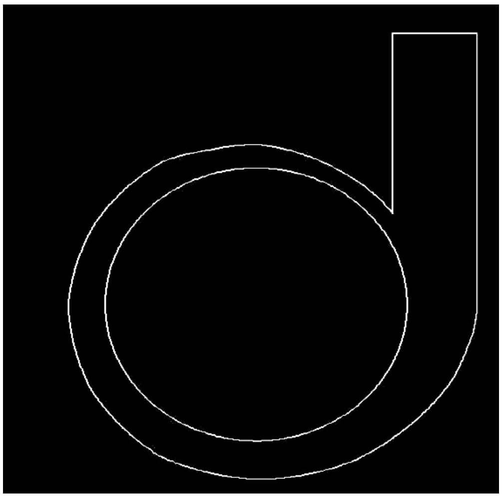

(b)

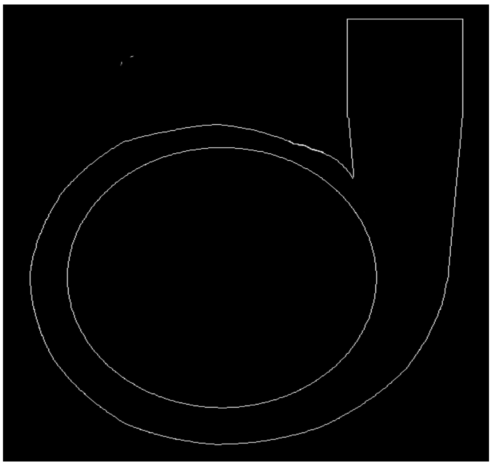

(c)

Figure 4.1: (a) existing design of the volute, (b) straight discharge design of the volute and (c) Slanted discharge design of the volute

Pagalthivarthi et al. (2011), suggests that a converging discharge tongue is more prone to abrasion of tongue wall and hence, accordingly hydraulic losses will be more. So, we have only increased the discharge slope and not taken the effect of decreasing its cross sectional diameter as it will only result into more hydraulic losses than the base casing design. Following Table 4.1 shows the outlet radius and outflow area of the three models:

Table 4.1: Outlet radius and area of the three models

Model	Outlet radius(mm)	Outlet area(mm^2)
Existing model	25	1963.5
Straight diffuser model	38	4536.5
Slanted diffuser model	50	7854

Computational Grid

The computational grid for the three models has been shown in Figure 4.2. Since, the grid test for the existing model has already been done in the previous work. Hence, the same grid size has been taken for the meshing of all the models.

Table 4.2: Grid information of the three models

Model	Grid number
Existing model	1400503
Straight diffuser model	1401274
Slanted diffuser model	1403797

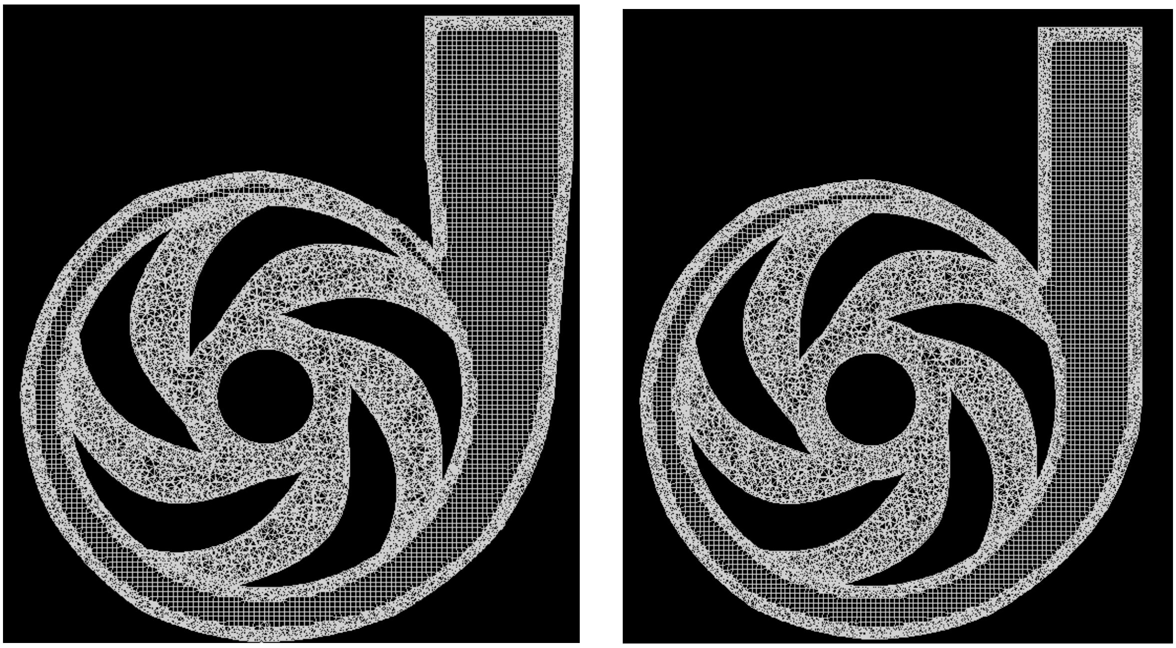

Figure 4.2: computational grid at mid span of the impeller of straight discharge and slanted discharge model

Simulation Setup

The commercial CFD package ANSYS Fluent 6.3.26 is used to perform the numerical simulations. The CFD code uses a finite volume approach to solve the model in hand. For all the models a steady and pressure based solver is used. Here for the analysis of single phase flow viscous model is used. The turbulence model selected is k- ε (two equations). For the pressure-velocity coupling SIMPLE algorithm is used. A moving reference frame condition is used for the rotational domain. Further, different boundary condition and descritization scheme is used accordingly for different domains. A convergence criterion of 1.0×10^{-4} is taken for all the simulations. All the boundary conditions are summarized in the following Table 4.3.

Table 4.3: Simulation Setup and Boundary condition for single phase analysis

Conditions	**Option**
Simulation model	3D
Solver	Pressure based, Steady
Discritization	First order
Single phase model	Viscous
Momentum	First order upwind
Turbulent kinetic energy	First order upwind
Turbulence dissipation rate	First order upwind
Convergence criterion	1.0×10^{-4}
Boundary conditions:	
Inlet	Velocity inlet
Outlet	Outflow
Inlet passage walls	No slip wall
casing walls	No slip wall
Impeller walls	Moving wall
Inlet passage zone	Stationary
Casing zone	Stationary
Rotating fluid zone	Moving reference frame

Here water is taken as the working fluid with viscous model. The properties of water is: ρ = 998.2 kg/m^3 and μ = 0.00100kg/m-s .

Results and Discussions

We have compared the results of the simulation of the three models at the midspan surface of the impeller-volute domain. The Figure 4.3 shows the pressure contours for the three models at 1450 rpm impeller rotational speed and (Q/Q_{BEP}=0.2)

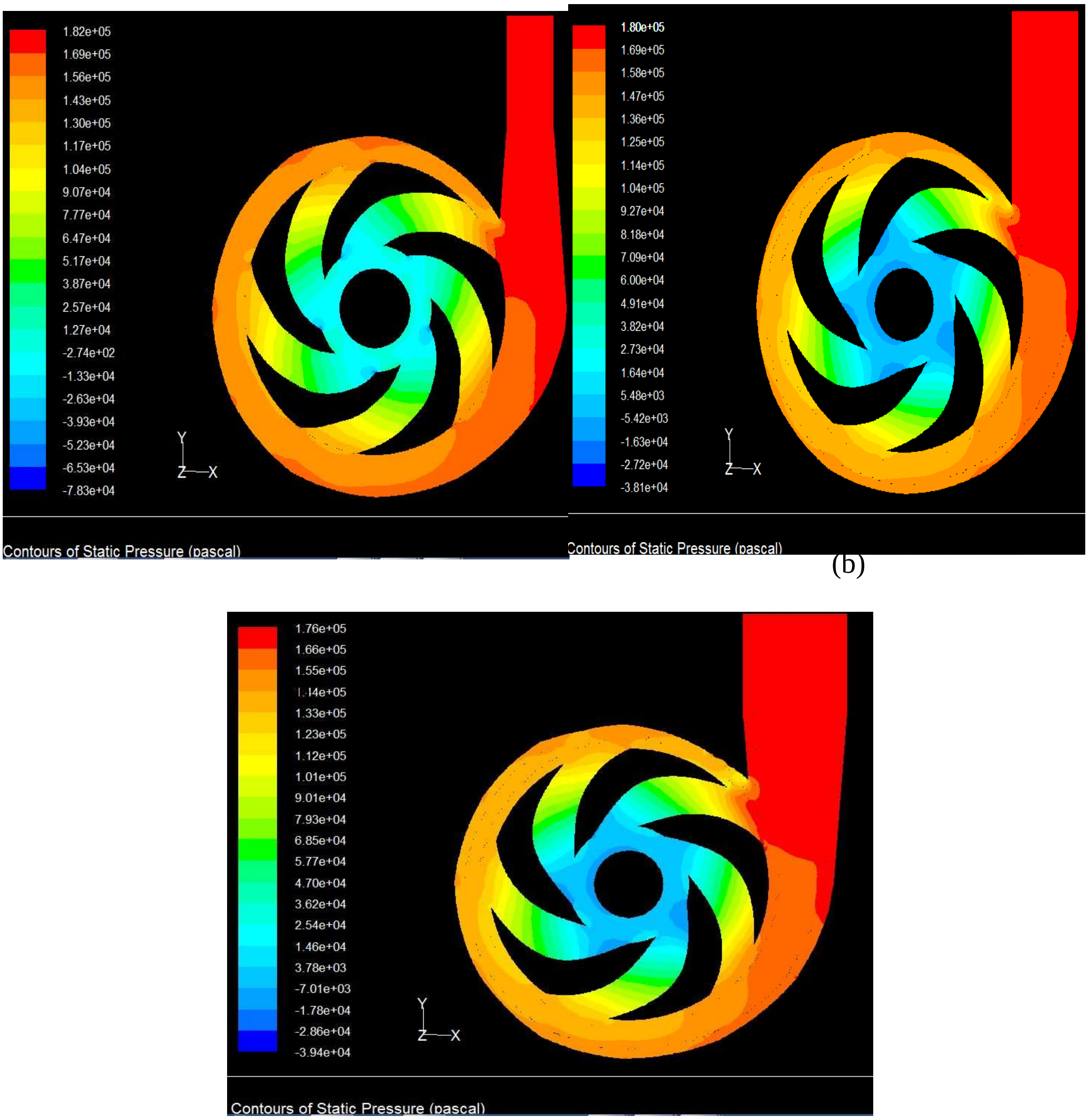

(c)

Figure 4.3: Pressure contour for (a) Existing model, (b) Straight discharge model and (c) Slanted discharge model at 1450 rpm and (Q/Q_{BEP}=0.2) for water

From the above Figure 4.3 it is very much clear that the pressure streamlines are more perpendicular to the blade passage wall in case of straight discharge as compared to the other two cases. Also, for the lower flow rate i.e. (Q/Q_{BEP}=0.2) the low pressure region at the screw section of the impeller hub i.e. at the inlet of the blades, is greater in case of straight and slanted discharge model of the volute tongue whereas in case of the existing model the low pressure region is quite small.

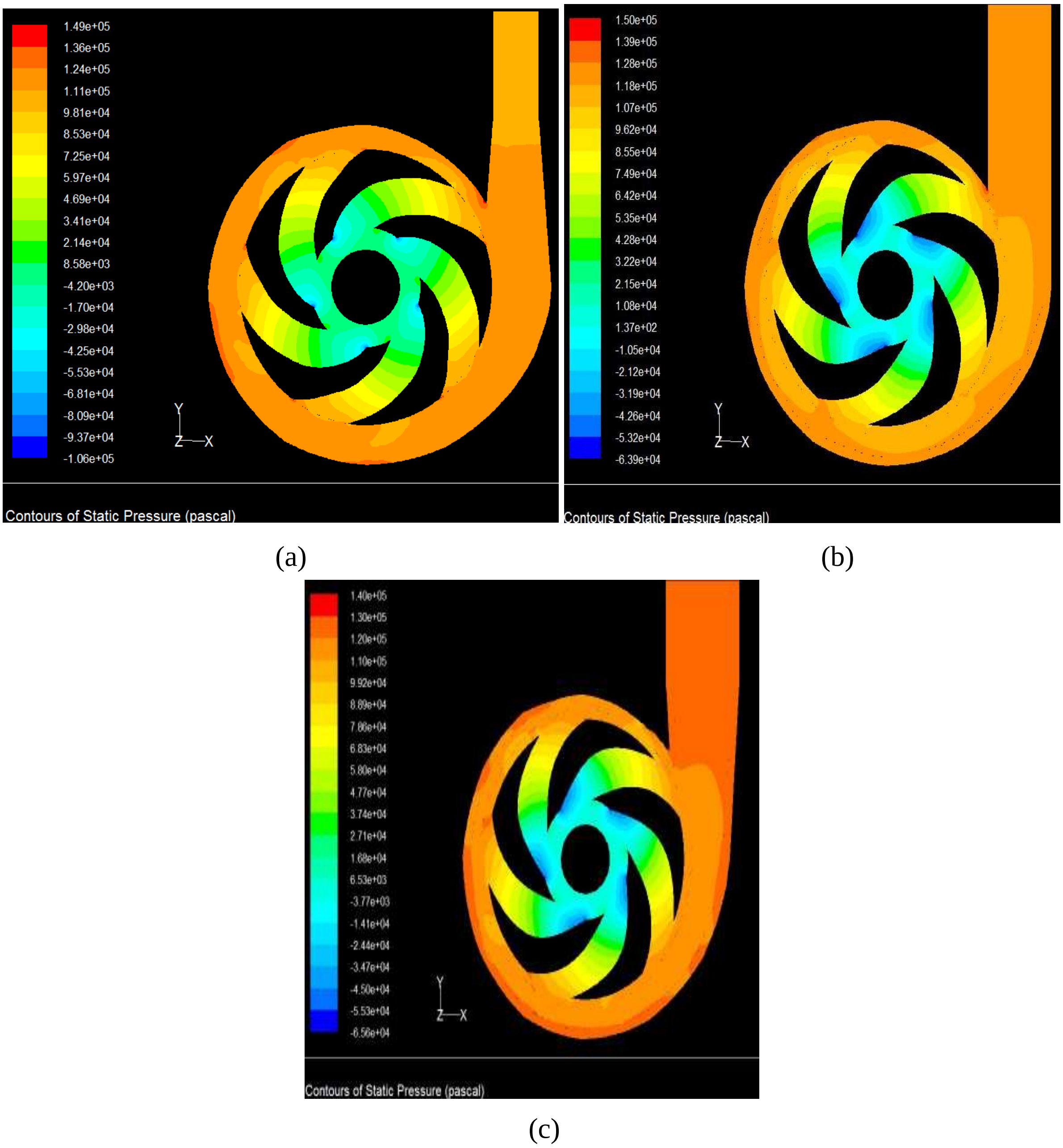

Figure 4.4: Pressure contour for (a) Existing model, (b) Straight discharge model and (c) Slanted discharge model at 1450 rpm and (Q/Q_{BEP}=1) for water

The Figure 4.4 shows the pressure contour for the three models at (Q/Q_{BEP}=1) at 1450 for water. It is evident from the diagram 4.4 that the straight discharge and the slanted discharge models are more capable of increasing the head in the tongue region. Also, there is a low pressure region at the outlet in the existing design whereas in case of straight discharge and slanted discharge models, there is no low pressure region evident.

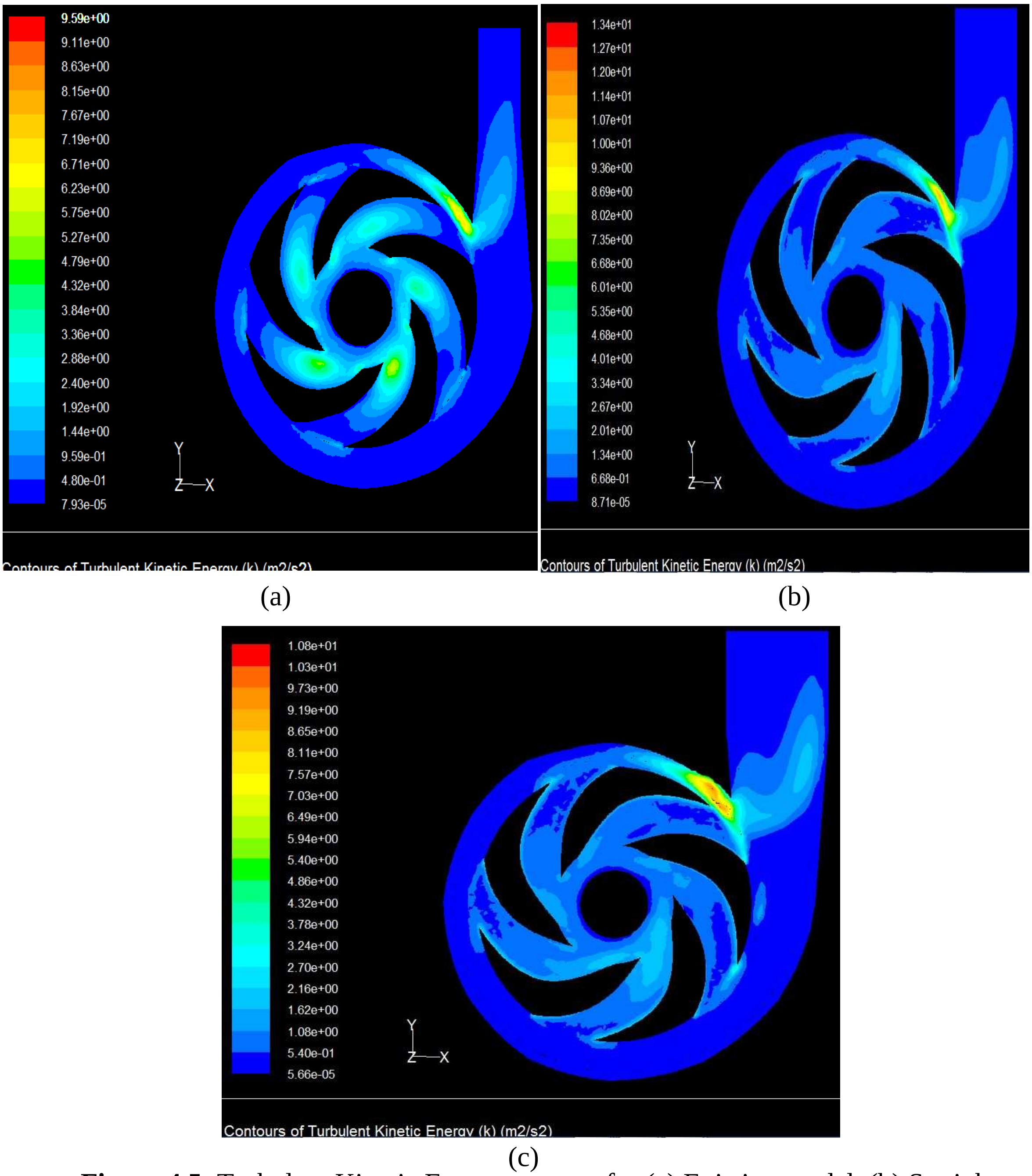

Figure 4.5: Turbulent Kinetic Energy contour for (a) Existing model, (b) Straight discharge model and (c) Slanted discharge model at 1450 rpm and (Q/Q_{BEP}=0.2) for water

Above Figure 4.5 shows the turbulence at the midspan of impeller-volute domain for (Q/Q_{BEP}=0.2) at 1450 rpm for water. It is very much evident from the Figure 4.5 that flow is much more turbulent in the blade passage region for the existing design and slanted discharge designs as compared to straight discharge design of the volute casing. However, in case of slanted discharge model the turbulence region at the cutwater is much greater than any other model.

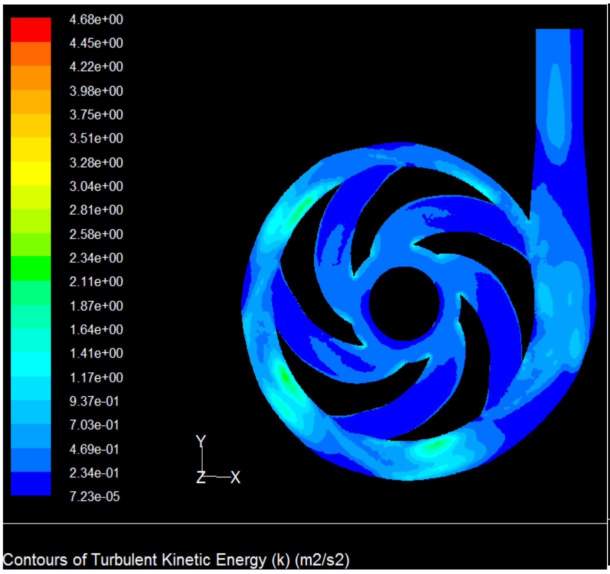

(a)

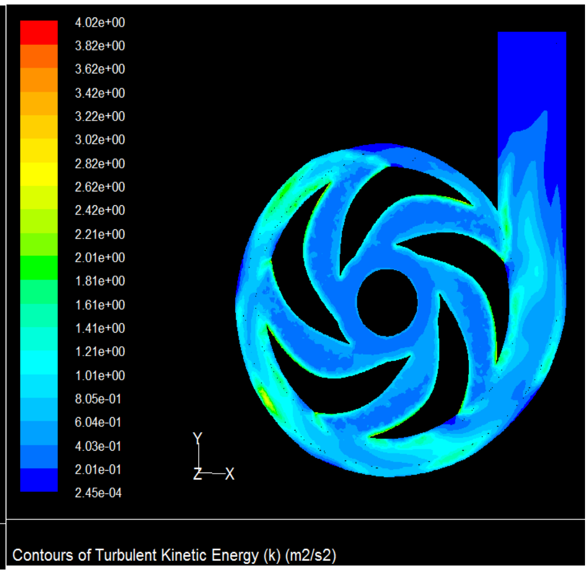

(b)

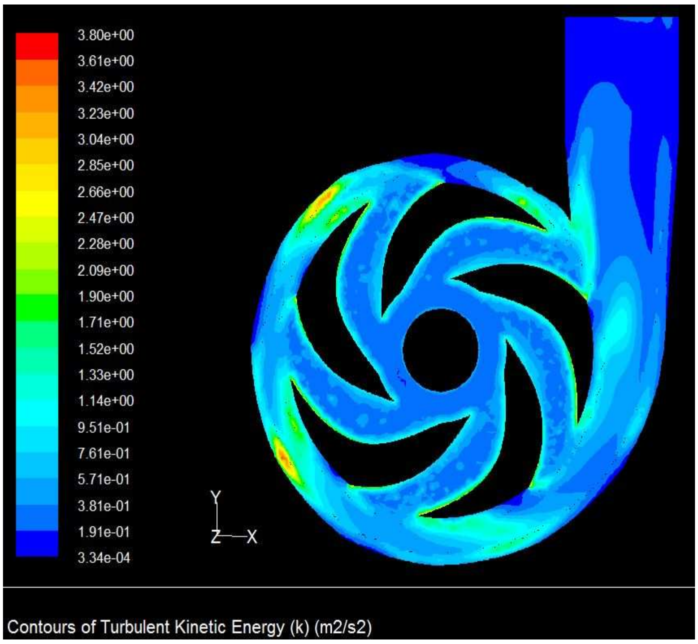

(c)

Figure 4.6: Turbulent Kinetic Energy contour for (a) Existing model, (b) Straight discharge model and (c) Slanted discharge model at 1450 rpm and (Q/Q_{BEP}=1) for water

The Figure 4.6 shows the turbulence kinetic energy contours at the midspan for (Q/Q_{BEP}) at 1450 rpm for water. There is a trurbulent flow region at the outlet of the tongue in the existing model and in case of slanted discharge model this turbulent region is quite small whereas, in case of straight discharge tongue model there is no turbulent region at the outlet. Also, the blade passageway is clear of any turbulent flow in case of straight discharge model.

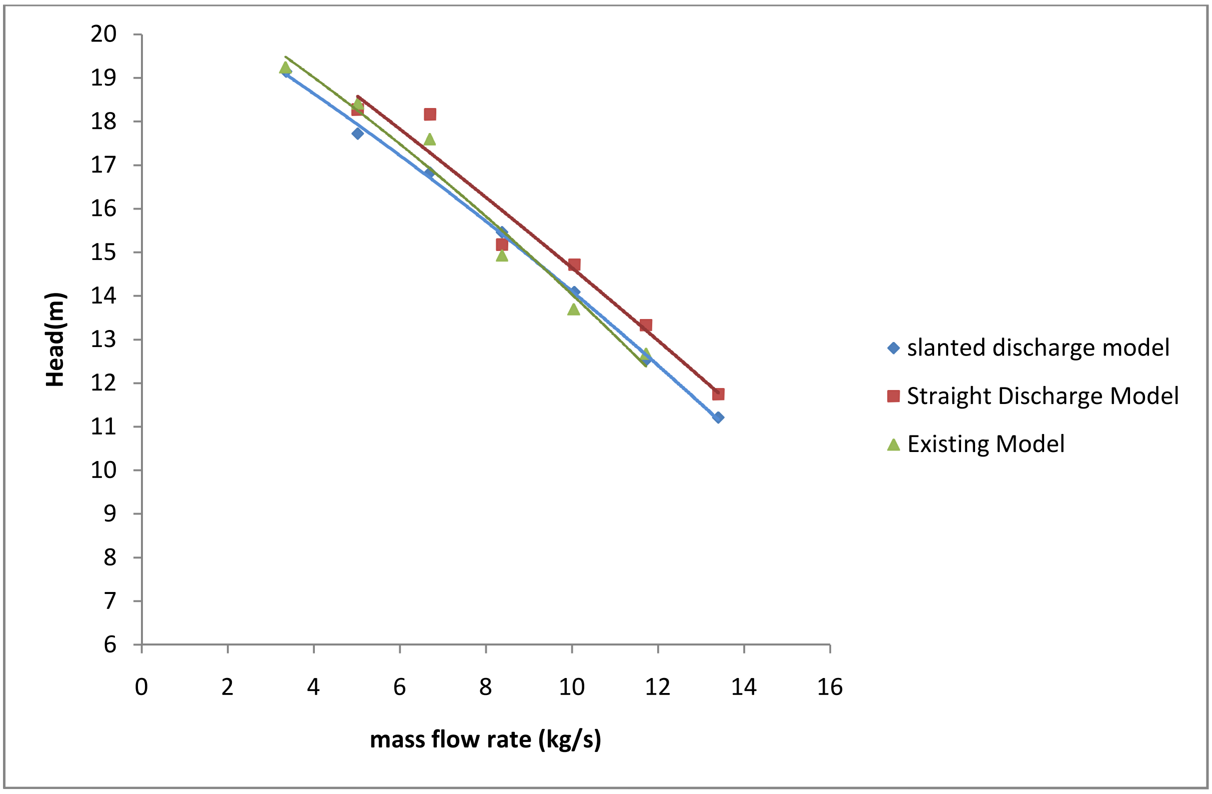

Figure 4.7: Head Vs Discharge plot for three models

Figure 4.7 shows the Head v/s Discharge curves for the three models. Here, we can see that the existing model has greater head than the slanted model, when away from the BEP. But, as soon as we move towards the BEP the Head curve for the slanted model moves up and gives greater head than the existing model. The Straight discharge model posses Head curve all the way above the Existing Model. Also it has been discussed in earlier section that the flow is more turbulent in case of Existing Model. So, it is evident from this fact that the Head curve is lower in case of Existing model as compared to the Straight discharge model. Further, the

Head curve for the Slanted discharge model surpasses the Head curve for the straight discharge model in the vicinity of BEP. So, overall, it can be considered that the straight discharge model is better of the later two.

4.1.2 CASE II: Effect of blending the cutwater region

In the earlier section we have already discussed how the flow happens at cutwater region when the pump is operating beyond BEP. So, in order to obtain a smooth recirculated flow towards the impeller belly region through the cutwater section the cutwater region has been rounded at a constant radius of 5 mm. The overall geometry of the pump remains almost same except at the cutwater section. For analyzing the effect of smoothened the cutwater region we have considered two models: existing model and straight discharge model from the previous section 4.1.1. As, in section 4.1.1, we have already observed that the straight discharge model is always better than the slanted discharge model. Hence, the slanted discharge model has not been taken for further improvement.

Computational domain and grid

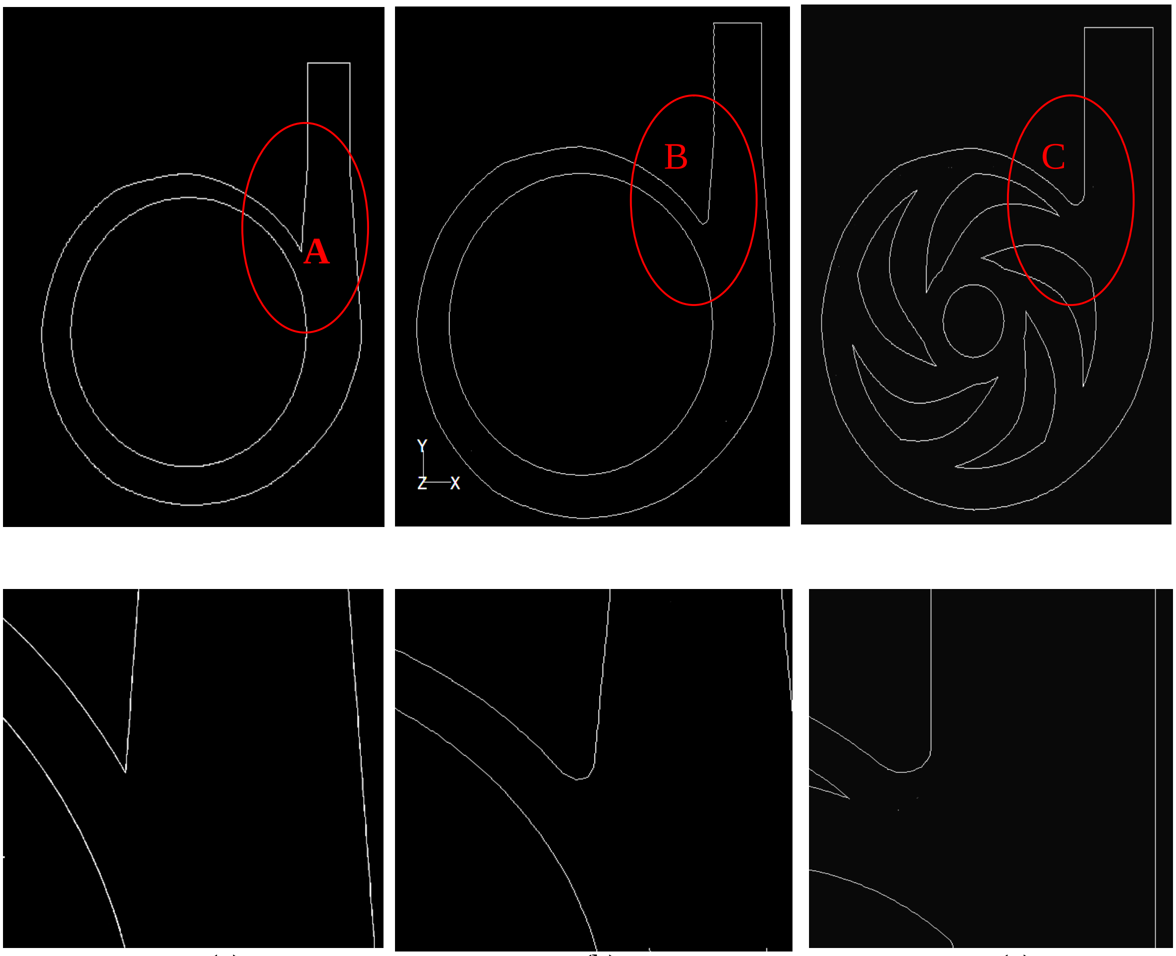

(a) (b) (c)

Figure 4.8: (a) Existing design of the volute, (b) Model 1(c) Model 2

The above Figure 4.8 shows the computational domain of the three cases: existing model, Model 1(existing model with blended cutwater) and Model 2(slanted discharge model with blended cutwater). In the model 1 and 2, the cutwater region is rounded (5 mm. constant radius) to accommodate smooth flow across it. Figure 4.9 shows the computational grid near the cutwater region in three cases.

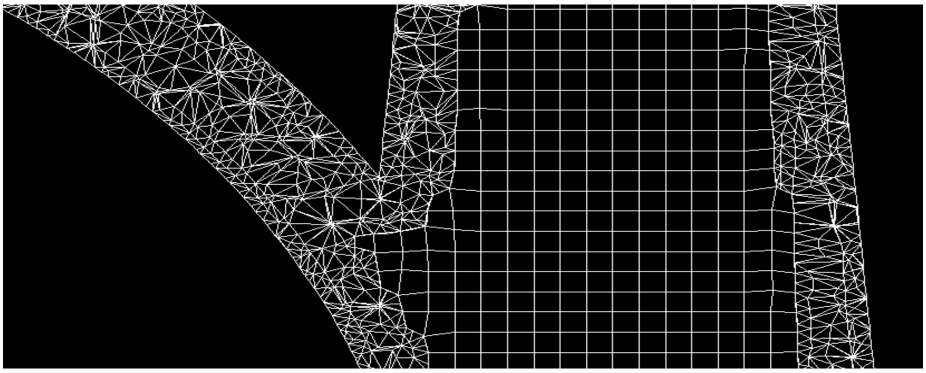

(a)

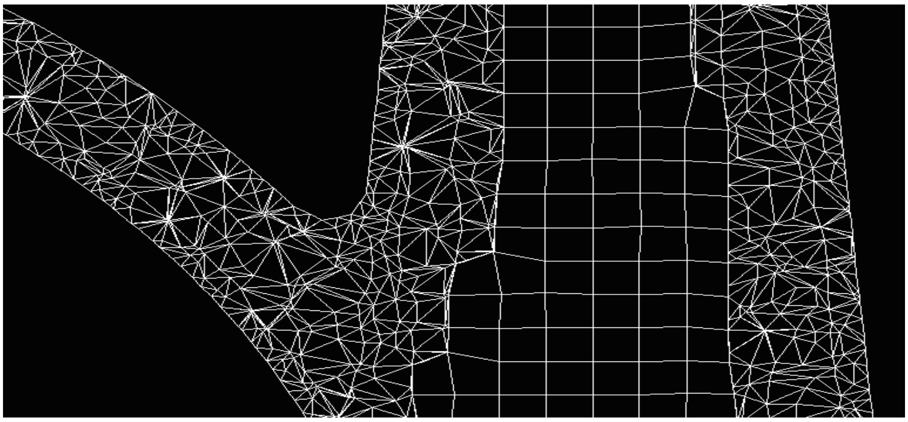

(b)

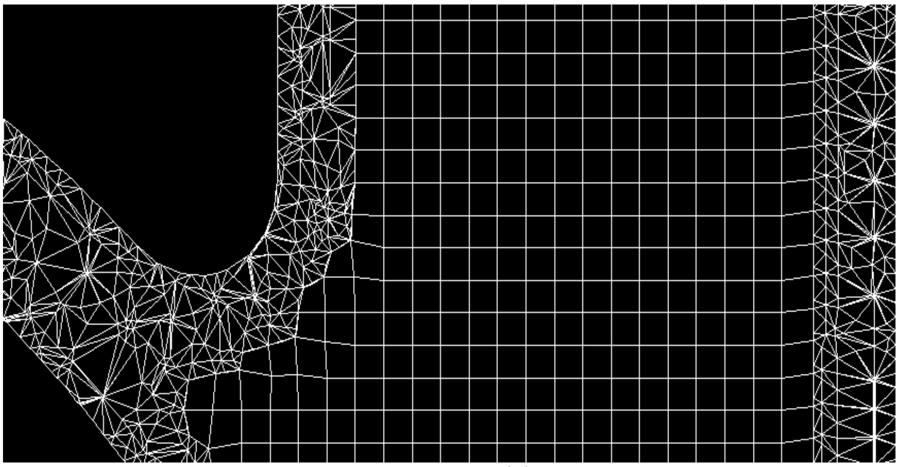

(c)

Figure 4.9: Computational Grid for (a) Existing Model (b) Model 1 (c) Model 2, near cutwater region

Simulation setup

The simulation setup is same as in case of Section 4.1.1. And the boundary conditions are given in Table 4.3.

Results and Discussions

The following Figure 4.10 shows the pressure contours for the existing model, Model 1 and Model 2 at (Q/Q_{BEP}=0.2) at 1450 rpm for water. We can see that model 2 has got higher static pressure at the outlet tongue region than both model 1 and existing model. Also, at the screw region of the impeller near the hub contains larger low pressure area in case of model 2.

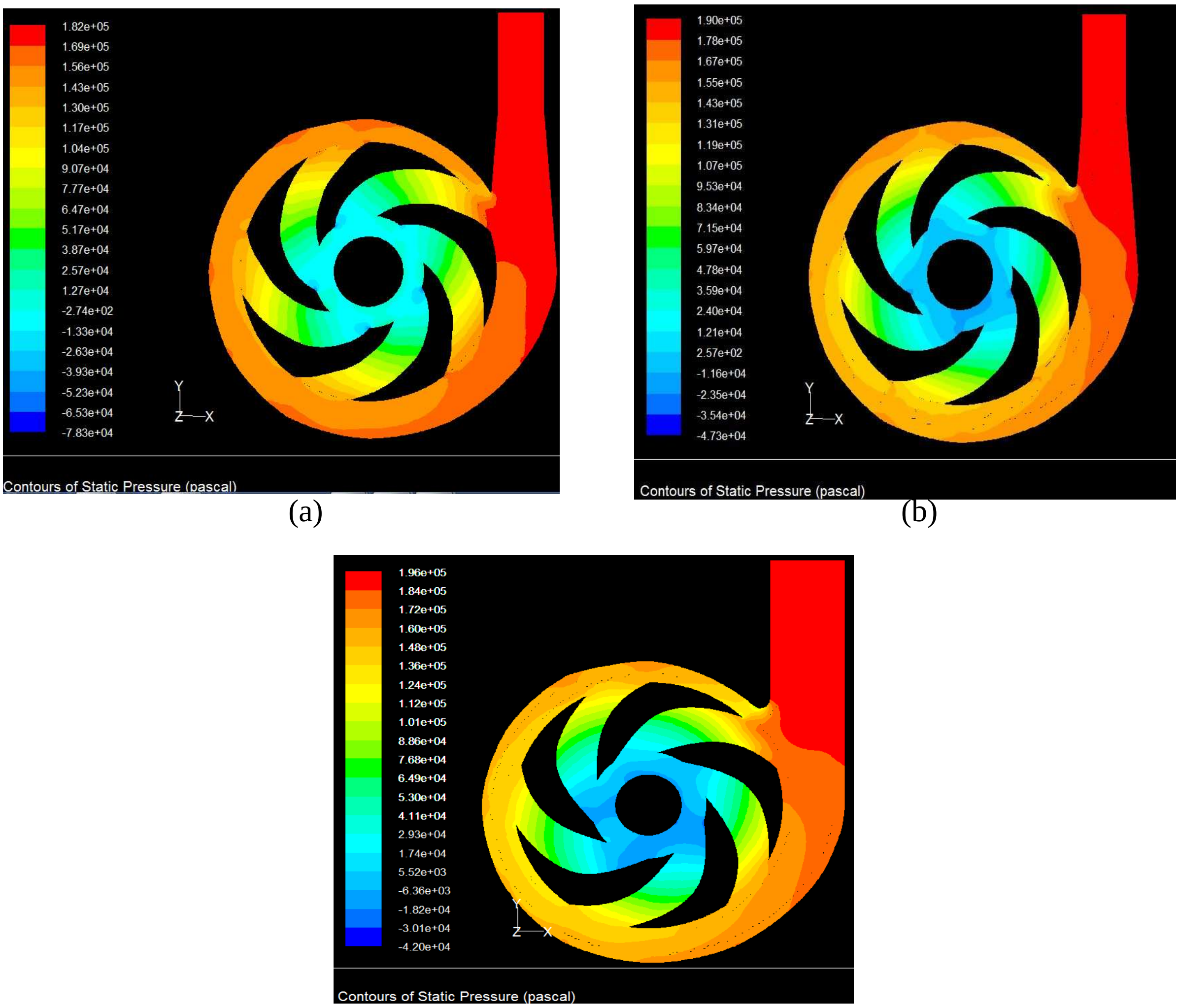

Figure 4.10: Pressure contour for (a) Existing model, (b) Model 1(c) Model 2, at 1450 rpm and (Q/Q_{BEP}=0.2) for water

Figure 4.11 shows the static pressure contour for the three models at (Q/Q_{BEP}=1) at 1450 rpm for water. It is evident from Figure 4.11 that the pressure streamlines are more uniform in case of model 2 as compared to both model 1 and existing model. There is a low pressure region at the outlet in case of: existing model and Model1. But, no such low pressure region has been seen with Model 2, and the span of this low pressure region is almost same in both cases. Also, in the Model 2, the value of static pressure at volute tongue is more than both the existing model and Model 1.

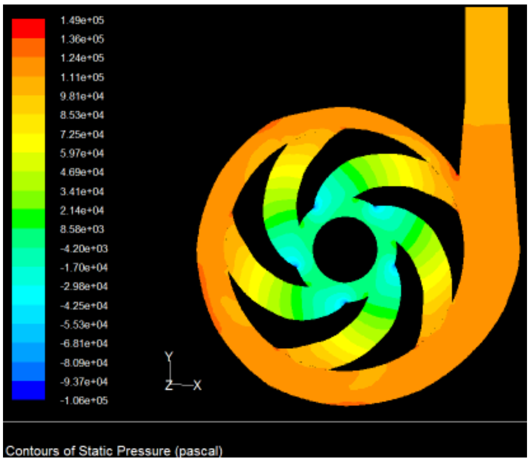

(a)

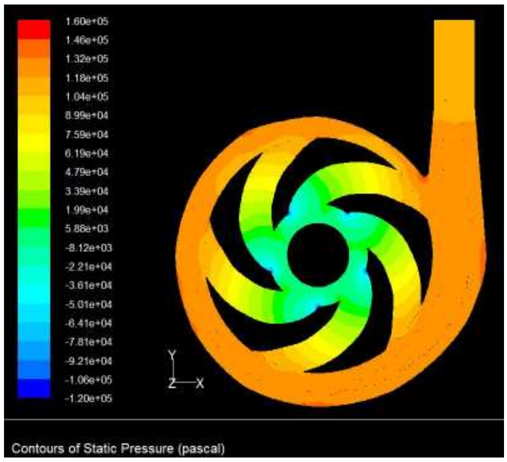

(b)

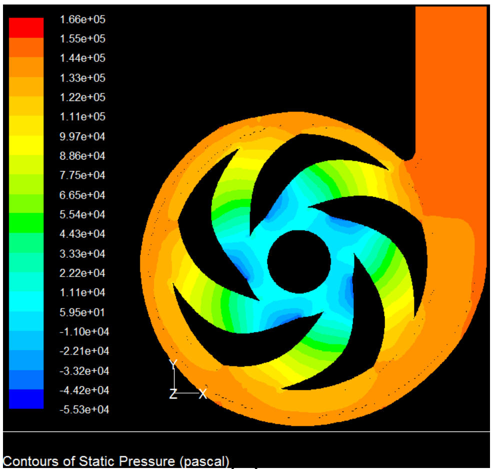

(c)

Figure 4.11: Pressure contour for (a) Existing model, (b) Model 1 and (c) Model 2 at 1450 rpm and (Q/Q_{BEP}=1) for water

Figure 4.12 shows the turbulence kinetic energy contour for the three models at (Q/Q_{BEP}=0.2) at 1450 rpm for water. From Figure 4.12 it is clearly evident that at the cutwater region, flow is very much turbulent for the existing model whereas in case of Model 1 and model 2, flow is not so turbulent around the cutwater region. Also, at the outlet tongue region there is no turbulent flow region seen in case of Model 1 and 2 as compared to the existing model, where appreciable amount of turbulence is available at outlet tongue region. Further, the existing

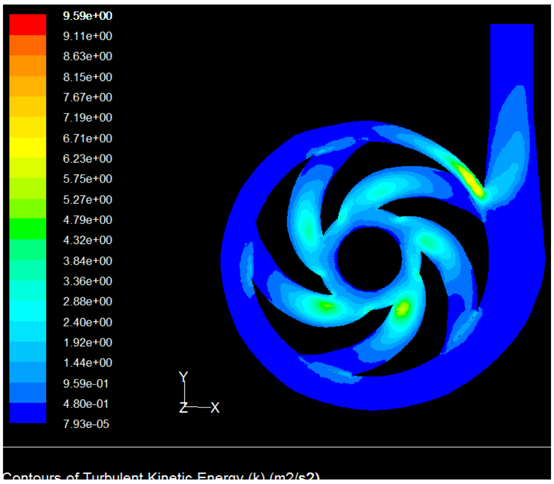

(a)

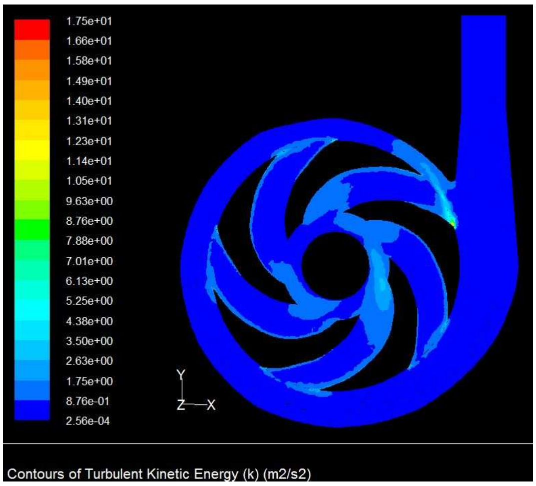

(b)

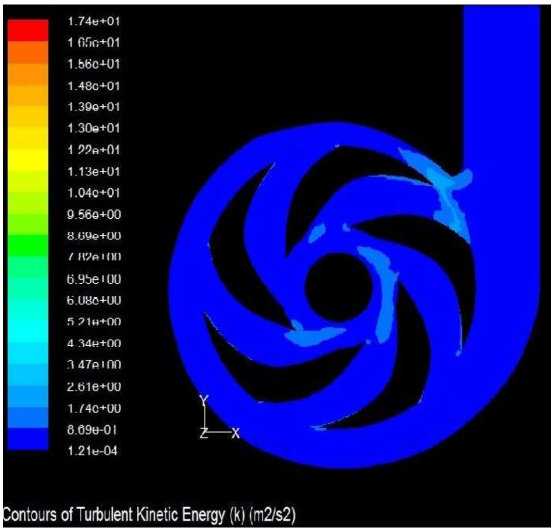

(c)

Figure 4.12: Turbulent Kinetic Energy contour for (a) Existing model, (b) Model 1 and (c) Model 2 at 1450 rpm and (Q/Q_{BEP}=0.2) for water

Model contains turbulent flow almost at every blade passage whereas, in case of model 1 and there is no turbulent flow seen throughout the blade passage.

Figure 4.13 shows the turbulent kinetic energy contour for the three models, at (Q/Q_{BEP}=1) at 1450 rpm for water. There is a turbulent flow region associated with the outlet section in case of Existing model whereas in Blended cutwater model no turbulence flow has been occurring at the outlet tongue. Also, the turbulence profile for the belly region of the volute casing is quite uniform in case of the Blended cutwater model as compared to the Existing model.

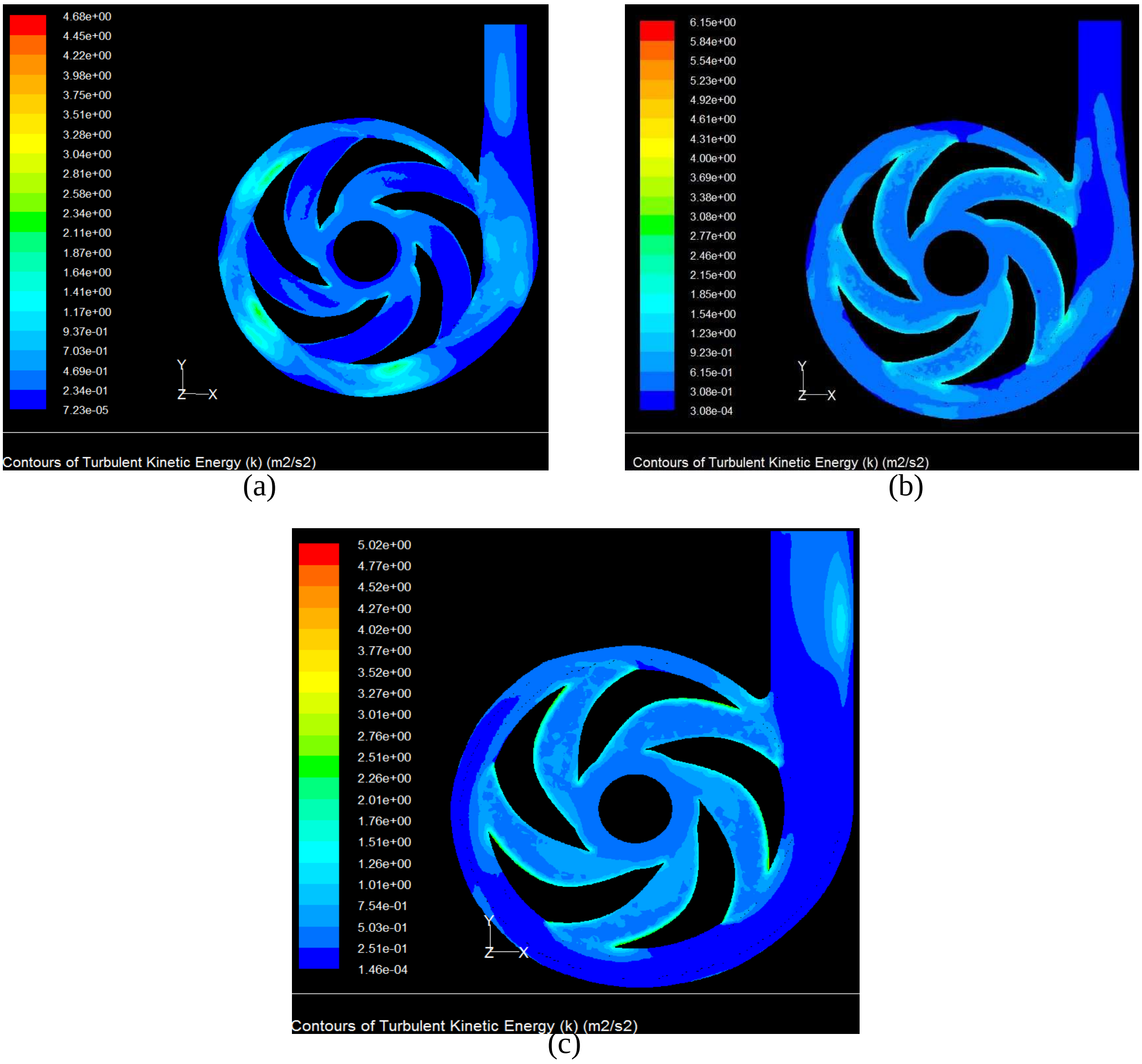

Figure 4.13: Turbulent Kinetic Energy contour for (a) Existing model, (b) Model 1 and (c) Model 2, at 1450 rpm and (Q/Q_{BEP}=1) for water

Figure 4.14 shows the velocity vector contour at the cutwater region for all three cases at 1450 rpm and at (Q/Q_{BEP}=0.2). It is clearly evident from the Figure 4.14 that the flow across the cutwater area is smooth in case of model 2 as compared to the Existing model and model 1. This flow has been affecting the pump performance appreciably at lower flow rates where there is recirculation flow across the cutwater area.

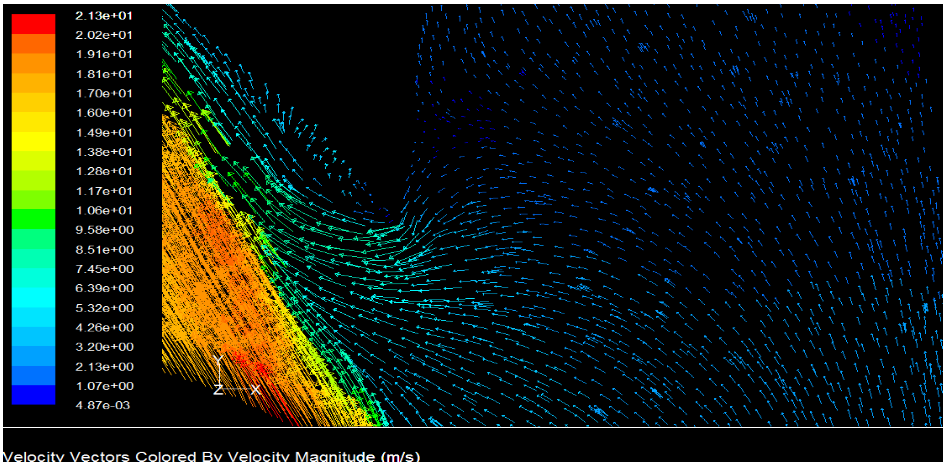

(a)

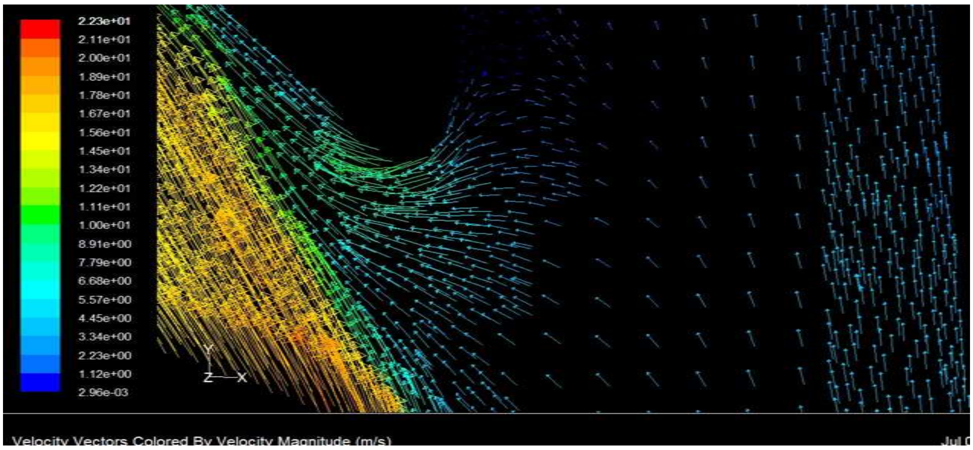

(b)

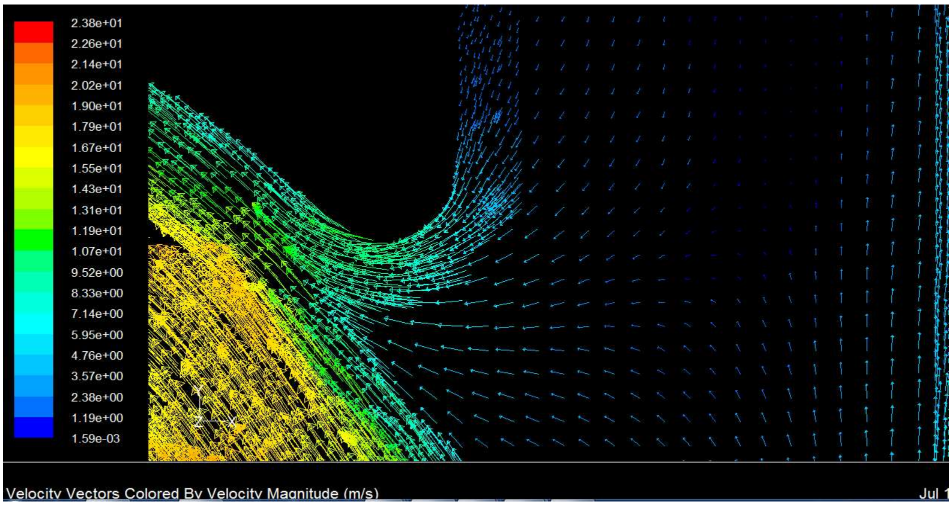

(c)

Figure 4.14: Velocity Vector contour at cutwater region (a) Existing model, (b) Model 1 (c) Model 2, at 1450 rpm and (Q/Q_{BEP}=0.2) for water

Figure 4.15 shows the Head Vs Flow rate curve of the three models with water at 1450 rpm. Cleary, the above given contours supports the results for the Head in the three cases. The end result is that the Model 2 posses a higher Head curve as compared to the Existing model and Model 1for all the flow rates.

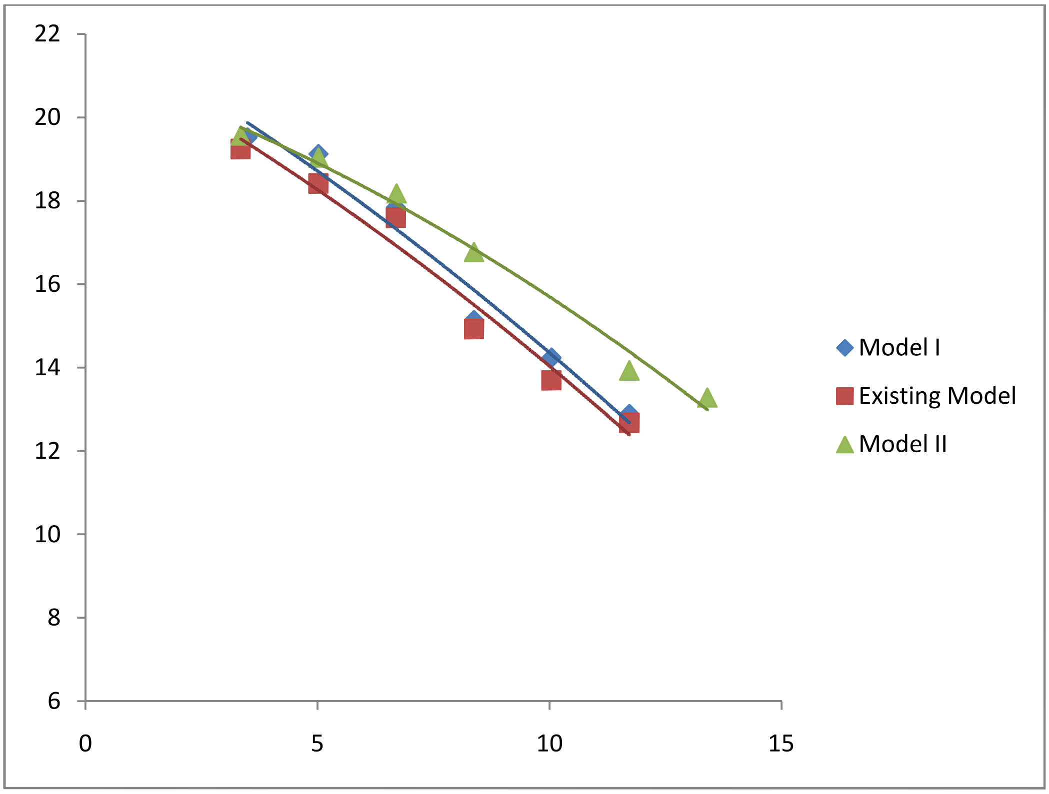

Figure 4.15: Head Vs Discharge plot for three models

4.2 MULTIPHASE FLOW ANALYSIS OF THE IMPROVED DESIGN

From the results of above section 4.1.2, we have found the improved design i.e. Model 2, of the pump. Now, we have been analyzing the improved geometry for multiphase analysis with Bottom Ash, as the secondary material. We have taken two concentrations of bottom ash (20% and 50% by weight) for the analysis at 1450 rpm.

Simulation Setup

For the multiphase flow analysis, Mixture model with granular secondary phase flow is used. The turbulence model selected is k- ε (two equations). For the pressure-velocity coupling

SIMPLE algorithm is used. A moving reference frame condition is used for the rotational domain. Further, different boundary condition and descritization scheme is used accordingly for different domains. A convergence criterion of 1.0×10^{-4} is taken for all the simulations. All the boundary conditions are summarized in the following Table 4.5. For the multi phase flow water is taken as the primary phase and bottom ash is taken as the secondary phase. The drag coefficient taken between two phases in case of is Schiller-Naumann, and for the slip velocity manninen-et-al model is used. The effect of lift is not considered for the present work. The restitution coefficient for the secondary phase collision is taken as 0.9. The properties of water and bottom ash are given in the table below:

Table 4.4: Material Properties

Water	Bottom ash
ρ = 998.2 kg/m^3	ρ = 2250 kg/m^3
μ = 0.00100kg/m-s	μ = 0.00476 kg/m-s
	Granular diameter = 0.16813 mm

Table 4.5: Boundary conditions

Conditions	**Option**
Simulation model	3D
Solver	Pressure based, Steady
Discritization	First order
Multiphase model	Mixture, 2-phase, implicit
Momentum	First order upwind
Turbulent kinetic energy	First order upwind
Volume fraction	First order upwind
Turbulence dissipation rate	First order upwind
Volume fraction	First order upwind
Convergence criterion	1.0×10^{-4}
Boundary conditions:	
Inlet	Velocity inlet
Outlet	Outflow
Inlet passage walls	No slip wall
casing walls	No slip wall
Impeller walls	Moving wall
Inlet passage zone	Stationary
Casing zone	Stationary
Rotating fluid zone	Moving reference frame

Results with Bottom ash

.First of all the simulation has been carried out with 20% (by weight) bottom ash concentration with the Model 2 and then concentration of bottom ash has been increased to 50% (by weight). The results for the two concentrations have been compared in both cases. Also, the volume fraction contours for the bottom ash have been shown.

Case I: Bottom ash concentration 20% (by weight)

Figure 4.16 shows the volume fraction and pressure contours for the existing design and improved design (Model 2) at 1450 rpm, 20% (by weight) bottom ash concentration at Q/Q_{BEP}=0.2

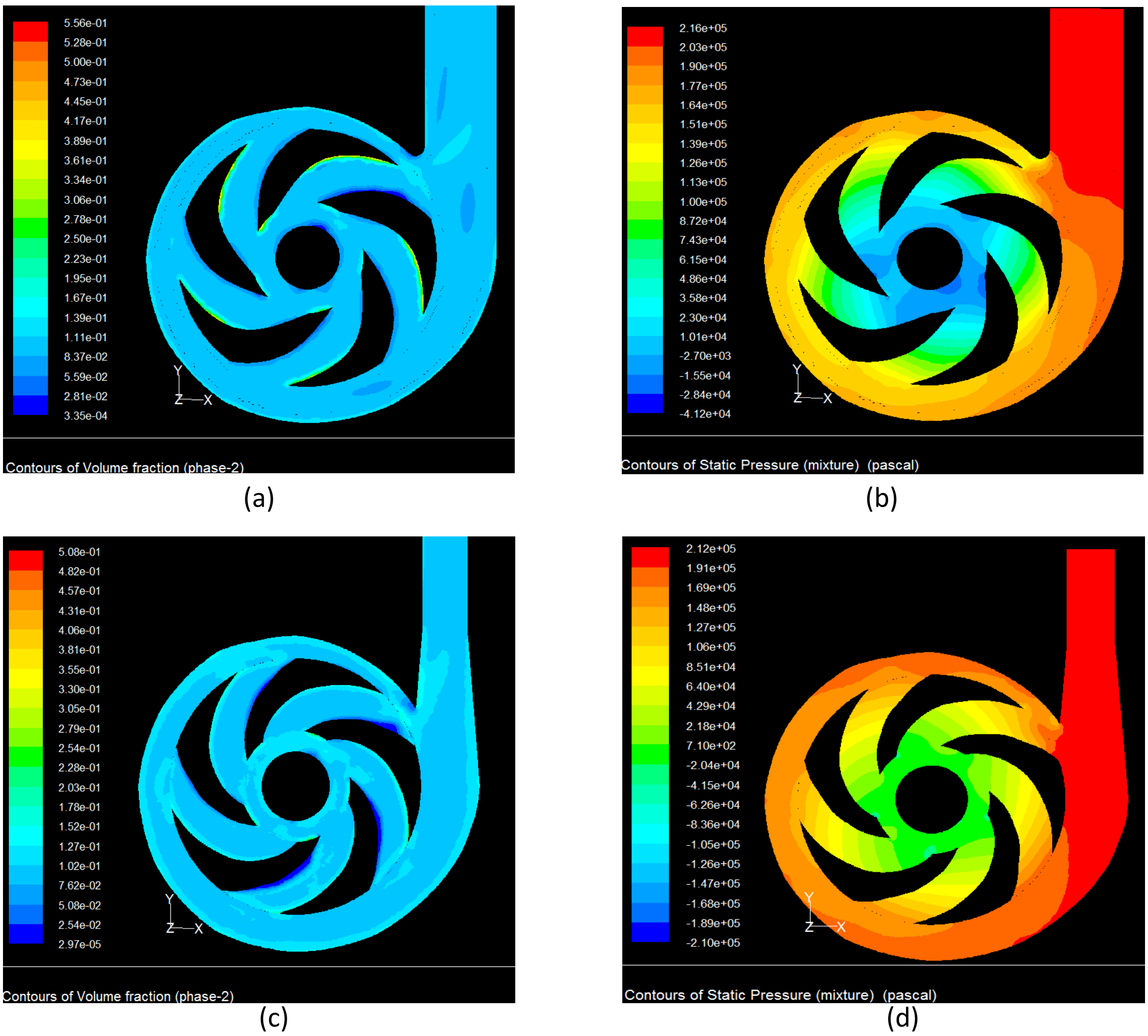

Figure 4.16: Volume fraction contour for (a) Improved Design (c) Existing Design and Pressure contour for (b) Improved Design (d) Existing Design at 1450 rpm, Q/Q_{BEP}=0.2 and concentration of bottom ash 20%(by weight)

From the solid volume fraction contours it is very much clear that solid particles are gathered more, near the hub and tongue region in case of existing design. Whereas, in case of improved design (Model 2) solids particles are flowing more uniformly and no gathering of solid particles has been seen. In the pressure contour for Model 2, we can see that there is a low pressure region at the screw section of the impeller. Also, the static pressure head at tongue is greater than the existing design of the pump.

Figure 4.17 shows the volume fraction and pressure contours for the existing design and improved design (Model 2) at 1450 rpm, 20% (by weight) bottom ash concentration at $Q/Q_{BEP}=1$

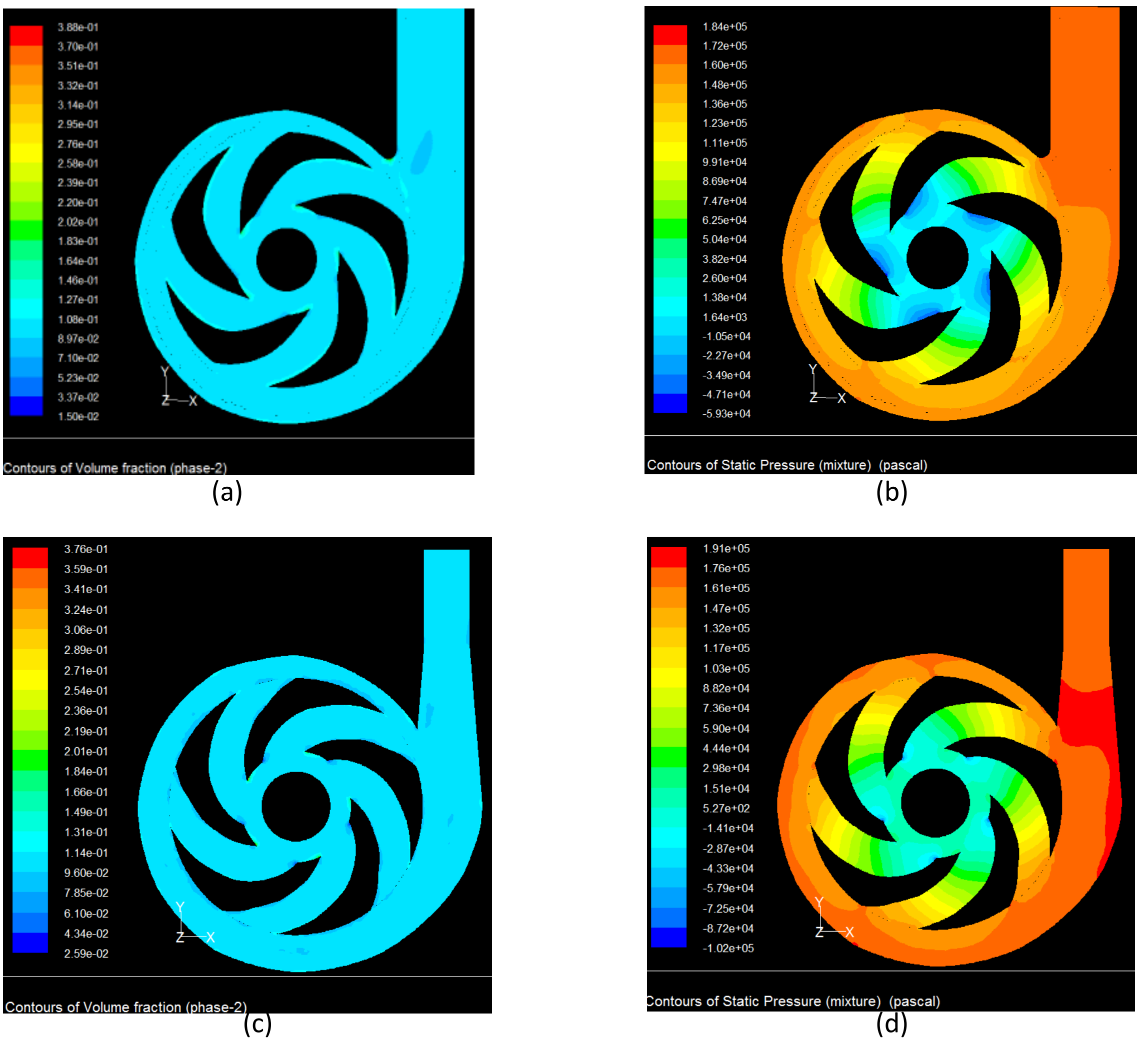

Figure 4.17: Volume fraction contour for (a) Improved Design (c) Existing Design and Pressure contour for (b) Improved Design (d) Existing Design at 1450 rpm, $Q/Q_{BEP}=1$ and concentration of bottom ash 20%(by weight)

From the solid volume fraction contours, for both the cases, namely: existing design and improved design, it has been observed that the flow is almost uniform and there is little difference in the distribution of the two. But from the pressure contours big differences can be seen, as in case of existing design there has always been a low pressure region associated with the outlet of the existing design. Whereas, in the pressure contours for improved design (Model 2) no such region is visible and the static pressure is greater than the existing design, in the outlet tongue.

CASE II: Results with Bottom Ash concentration 50% (by weight)

Figure 4.18 shows the volume fraction and pressure contours for the existing design and improved design (Model 2) at 1450 rpm, 50% (by weight) bottom ash concentration at Q/Q_{BEP}=0.2.

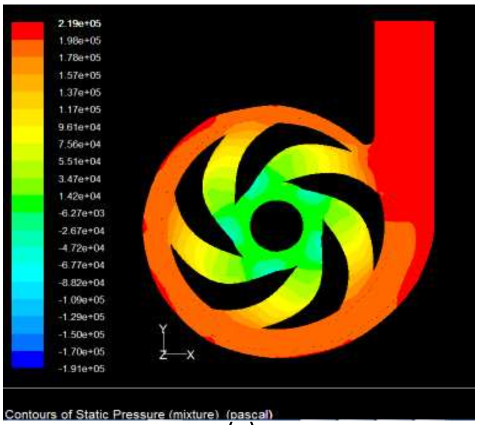

(a)

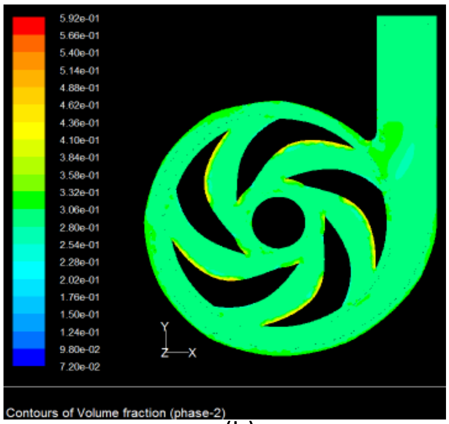

(b)

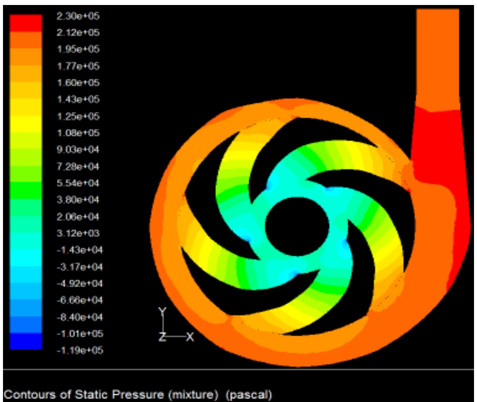

(c)

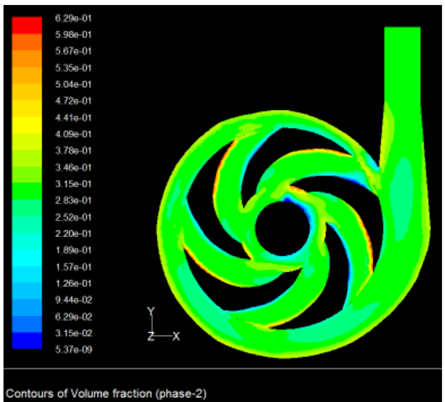

(d)

Figure 4.18: Pressure contour for (a) Improved Design (c) Existing Design and Volume fraction for (b) Improved Design (d) Existing Design at 1450 rpm, Q/Q_{BEP}=0.2 and concentration of bottom ash 50%(by weight)

From the above Figure 4.18 it is clearly visible that flow of solid particles are more uniform in case of improved design as compared to the existing design. Whereas, in case of existing design solid particles have a tendency to gather near the hub and walls of the volute tongue. Also, there is a low pressure region associated with the outlet in case of existing design. While, the static pressure streamlines are rather uniform in case of improved design (Model 2). Also, the static pressure is increasing uniformly towards the outlet in case of Model 2.

Figure 4.19 shows the volume fraction and pressure contours for the existing design and improved design (Model 2) at 1450 rpm, 50% (by weight) bottom ash concentration at $Q/Q_{BEP}=1$.

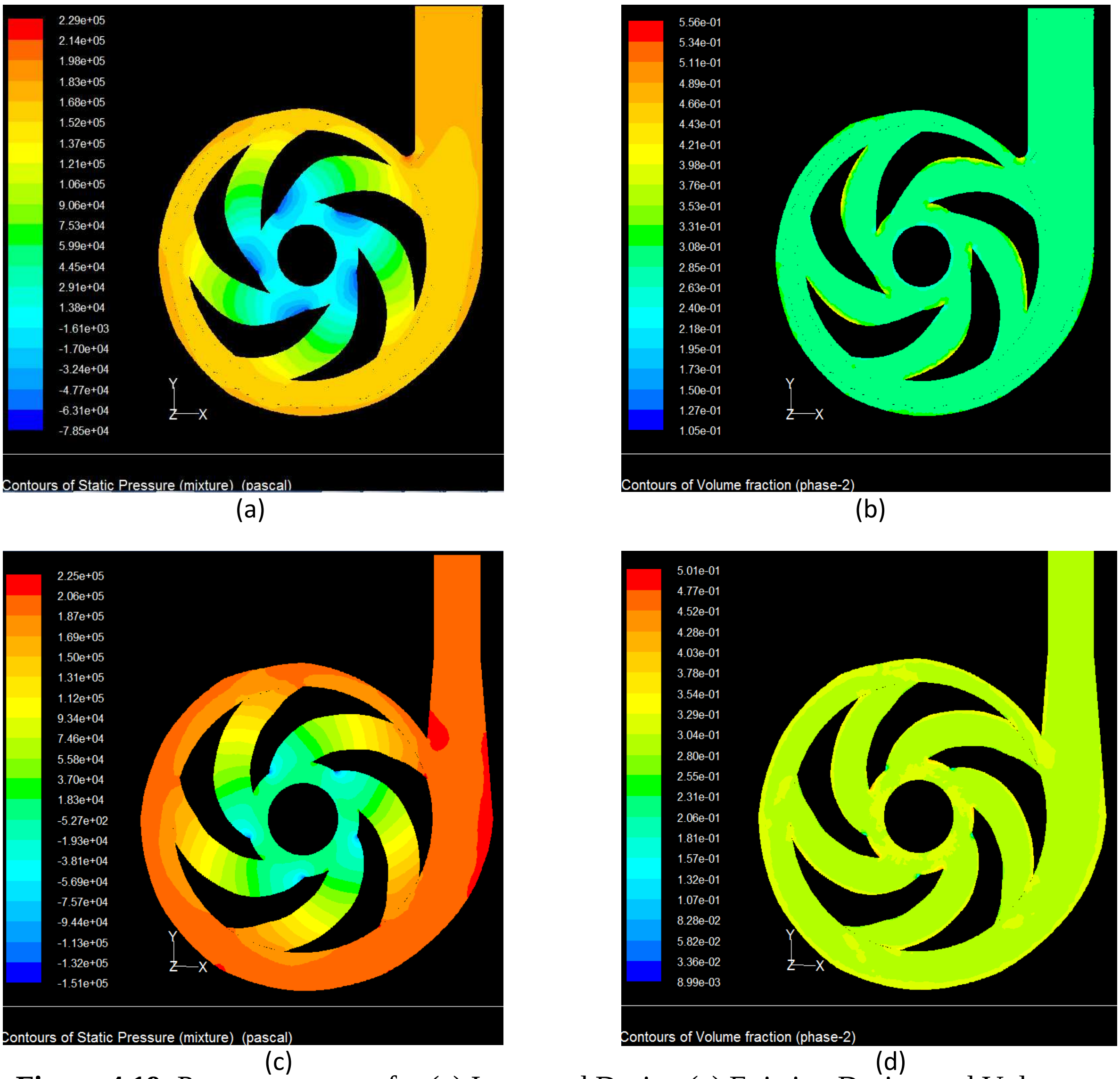

Figure 4.19: Pressure contour for (a) Improved Design (c) Existing Design and Volume fraction for (b) Improved Design (d) Existing Design at 1450 rpm, $Q/Q_{BEP}=1$ and concentration of bottom ash 50%(by weight)

From the volume fraction contours of Figure 4.19 we can see that the solid volume fraction contour is more uniform in case of the Improved design (Model 2) than the existing design. While in case of existing design it can be seen that there are many regions where the solid particles are sticking to the wall and interfaces. Also, from the pressure contour of existing design, we can see that the static pressure is not increasing uniformly in the volute region, rather local high pressure region has been observed in the volute region. But, in case of improved design, the static pressure streamlines are more uniform.

Figure 4.20 shows the pressure head for the improved design for water, 20 % and 50 % bottom ash concentrations.

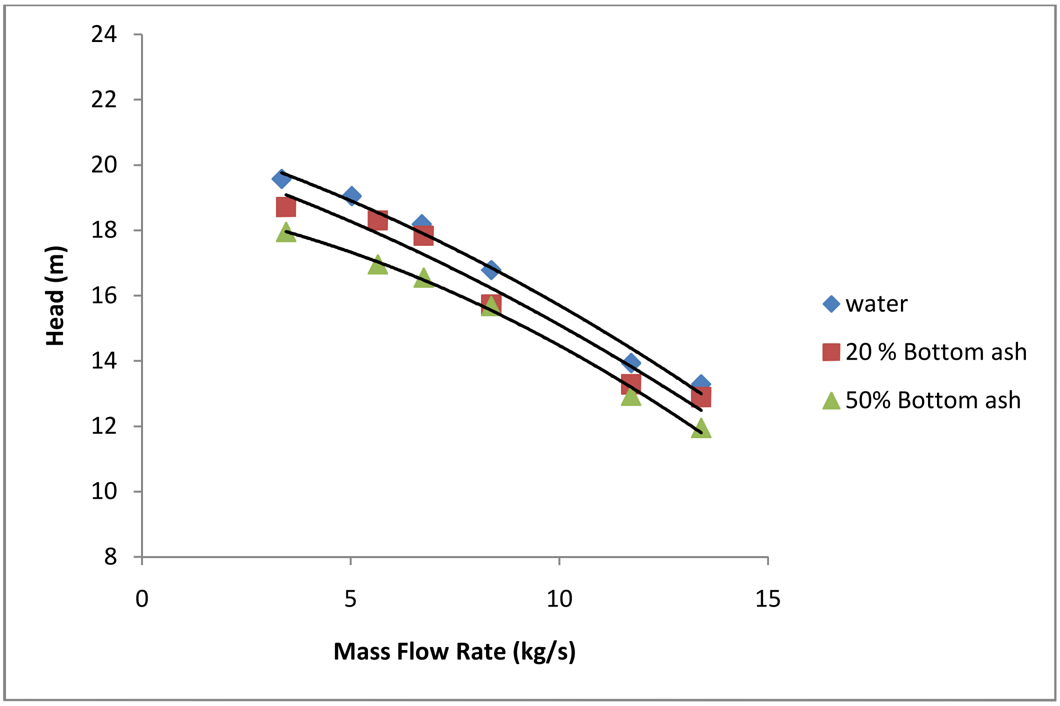

Figure 4.20: Head Vs Flow rate plot for the improved design with water, 20% and 50% bottom ash at 1450 rpm and different flow rates

From the above figure it is clearly visible that the head is decreasing as the concentration of the bottom ash increases in the slurry.

4.3 CONCLUSION

Model 2 has been obtained as the final improved design. It is performing better than the existing design of pump in case of water and slurry flow at almost all the flow rates. Also the flow around the cutwater region is smoother than the previous design.

CHAPTER 5 PERFORMANCE OF PUMP WITH VARIATION IN BLADE NUMBER

In this chapter the modeling of impeller with different blade numbers (4, 5 and 6) is discussed and the computational results obtained with different impellers are compared with the original design having number of blades- 5.

For the purpose of numerical analysis on the pump with different impeller designs, the dimensions of the existing pump are required to generate a model in the software. Modeling and analysis of existing pump with blade number 5 was already done. So, in order to make design improvements first of all the results and contours of previous computational analysis (22) is thoroughly studied and then new designs were suggested with the existing pump (blade number 5) in Chapter 4. And the effect of different blade numbers on overall pump performance has been studied in this chapter by taking comparisons of the computational data of blade numbers: 4, 5 and 6.

5.1 MODELING OF PUMP WITH DIFFERENT BLADE NUMBER

All the parts of the existing pump is same for the models with 4 and 6 blade, only the impeller is different.

Impeller

The existing centrifugal pump contains the impeller with blade number 5 and is of enclosed type. As the model of the existing pump impeller with blade numbers 5 was already done, so impellers with blade numbers 4 and 6 is modeled using the principle blade design of the existing pump with GAMBIT software. Figure 5.1 shows the impeller with different blade numbers.

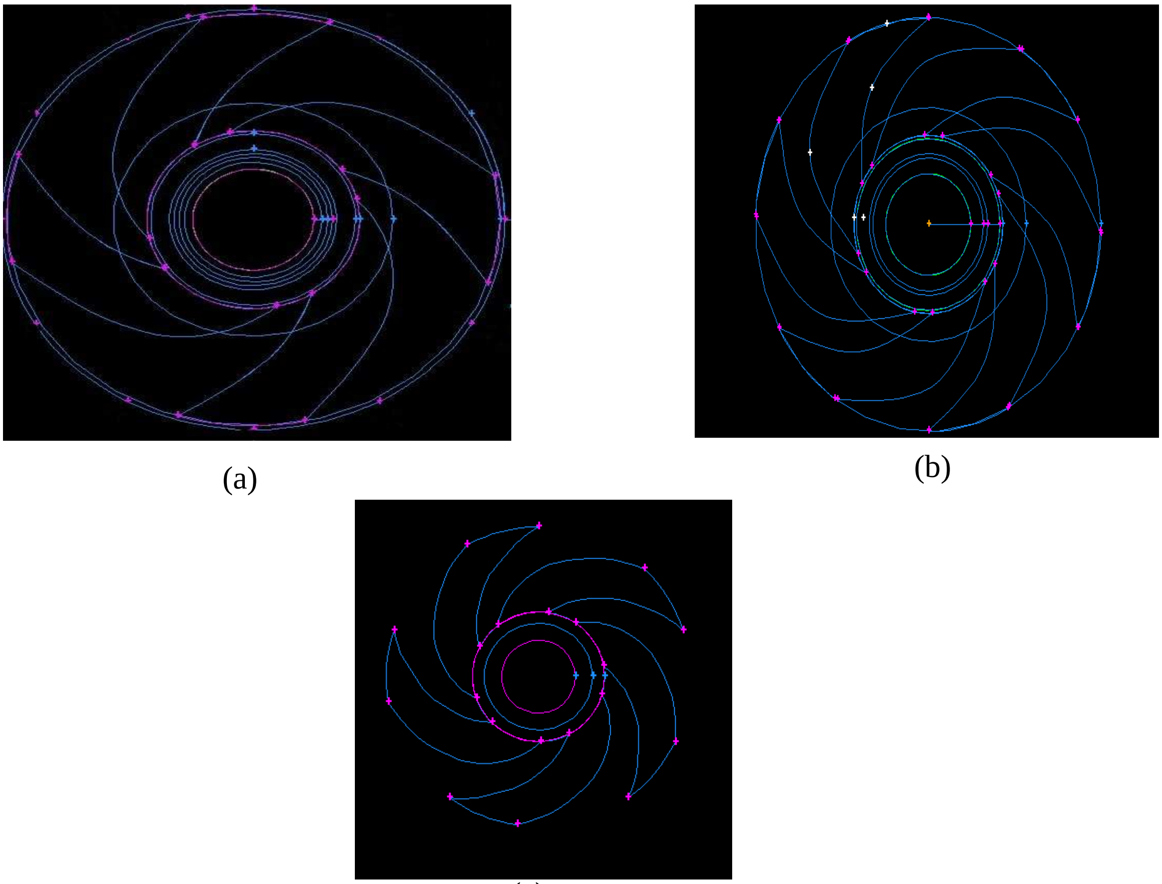

(a) (b) (c)

Figure 5.1: impeller design (a) 4 blade (b) 5 blade and (c) existing model with 5 blades

Other components are designed as per the method explained in Chapter 3.

Meshing

The meshing is done on the GAMBIT 2.3.16 package. A tetrahedral-hex core meshing is done for all the components of the centrifugal slurry pump. Fine meshing is done for the regions were the forces are more significant and coarser meshing size function is used for all other regions. A grid sensitivity test is also done for the models with blade number 4 and 6 as the model with blade number 5 was already taken after grid sensitivity testing. As far as the analysis of the pump is concerned a finer meshing scheme is used to take in consideration of the every vital fact which is affecting the flow in case of single as well as multi-phase flow. Following picture shows the computational grid at mid plane of the pump.

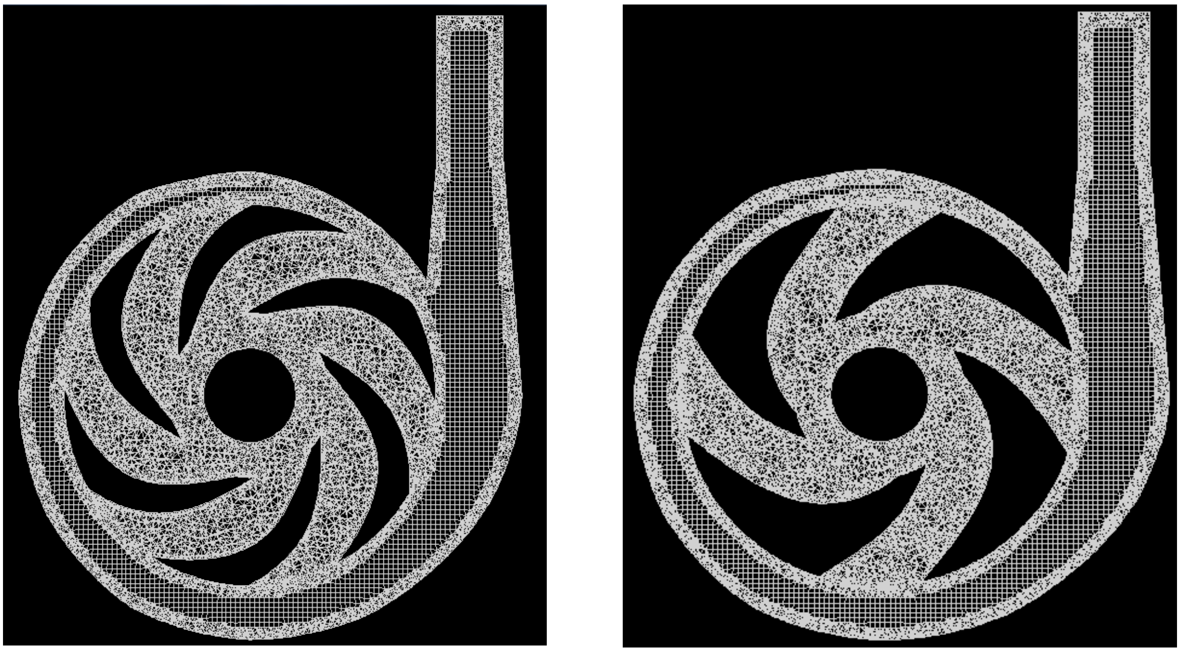

(a) (b)

Figure 5.2: computational grid for (a) 6 blade model and (b) 4 blade model

5.2 SIMULATION SETUP

The commercial CFD package ANSYS Fluent 6.3.26 is used to perform the numerical simulations. The CFD code uses a finite volume approach to solve the model in hand. For all the models a steady and pressure based solver is used. Here for the analysis of single phase flow viscous model is used. The turbulence model selected is k- ε (two equations). For the pressure-velocity coupling SIMPLE algorithm is used. A moving reference frame condition is used for the rotational domain. Further, different boundary condition and descritization scheme is used accordingly for different domains. A convergence criterion of 1.0×10^{-4} is taken for all the simulations. All the boundary conditions are summarized in the following Table 4.2.

5.3 GRID INDEPENDENCY TEST

The grid independency check at the BEP has been done for the two models (4 bladed and 6 bladed), in this section.

Grid Independency Test for 4 Bladed Model

Table 5.1: Grid Independency Test for 4 bladed design

Grid Size	Total Elements	No. of tetrahedral elements	No. of hexahedral elements	Head
4	973403	815990	157413	10.52
3.5	1111090	953669	157421	10.48
3.25	1194478	1037057	157421	10.47
3	1297763	1140328	157435	10.47

Grid Independency Test for 6 Bladed Model

Table 5.2: Grid Independency Test for 4 bladed design

Grid Size	Total Elements	No. of tetrahedral elements	No. of hexahedral elements	Head
4	924788	766703	158085	14.31
3.5	1103224	945135	158089	14.29
3.10	1238115	1080020	158095	14.27
3	1354292	1196191	158101	14.27

5.4 RESULTS AND DISCUSSIONS

In this section, first of all, the simulation results for the 3 models has been discussed with water, as the working fluid and further, results has been discussed for the multiphase physics.

Results with Water

Single phase physics has been applied with the models of pump with blade number: 4 and 6 at BEP and the data has been compared with the Existing model i.e. pump with blade number=5.

Figure 5.5 shows the pressure contours with water at 1450 rpm and Q/Q_{BEP}=1 in case of the three models

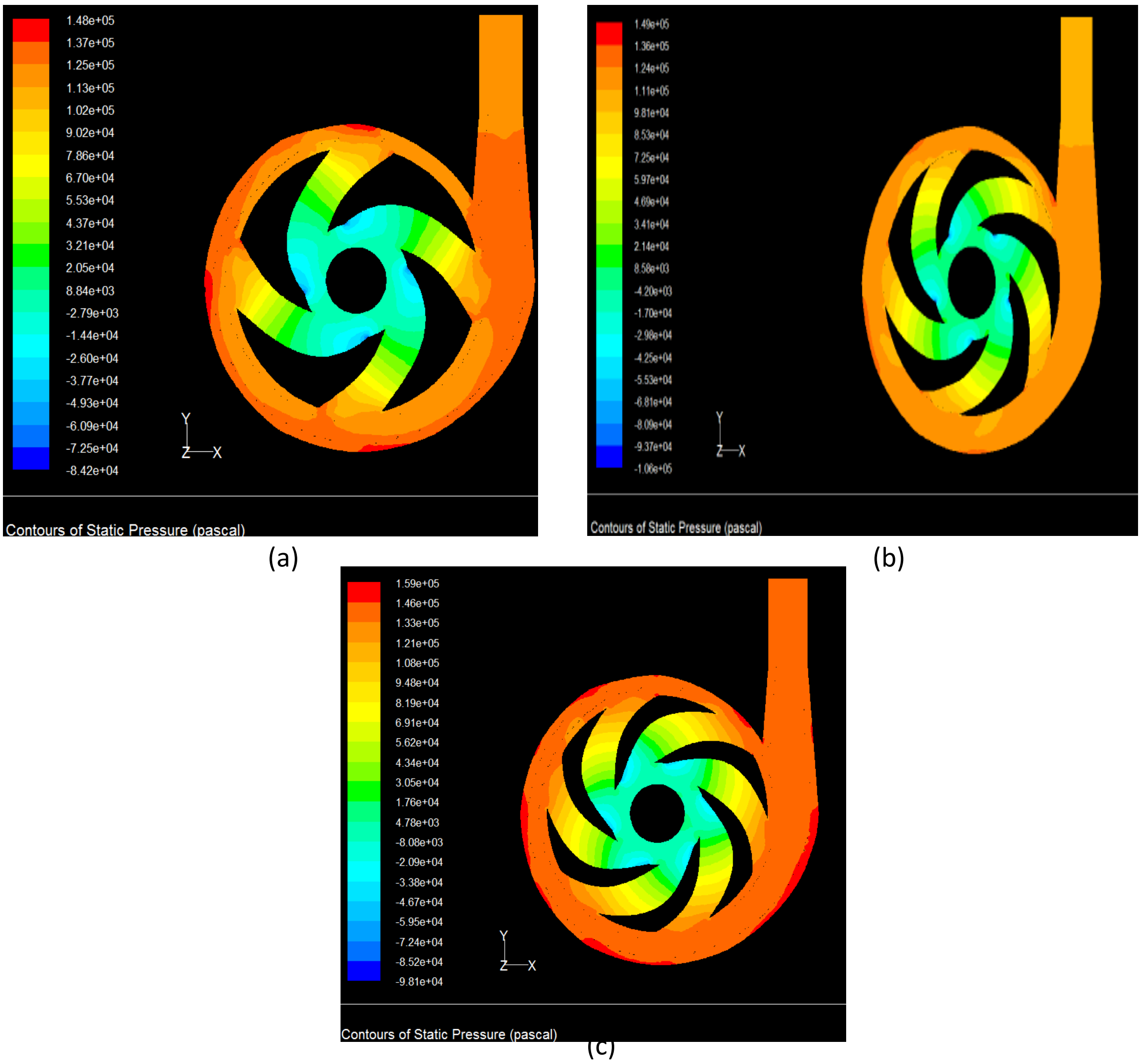

Figure 5.3: pressure contour for (a) 4 blade (b) 5 blade and (c) 6 blade model at 1450 rpm and Q/Q_{BEP}=1 with water

From the Figure 5.5 it is very much clear that the 4 bladed design is generating less head as compared to the two other models with blade number 5 and 6. Also, the static pressure stream lines are more uniform in case of 5 and 6 bladed designs. There is a low pressure region associated with outlet surface in case of four bladed and five bladed designs. But, the 6 bladed design is producing more head than the 5bladed design. So, for further analysis to optimize the blade number cannot be performed before considering the effect of higher blade numbers.

5.5 CONCLUSION

Further analysis cannot be performed without optimizing the blade numbers. As, we have got greater head for the 6 bladed design than the existing 5 bladed design. Hence, further analysis can only be performed when the optimized blade number is available. For optimizing the blade number, effect of higher blade number should also be considered.

CHAPTER 6 CONCLUSION AND FURTHER SCOPE

6.1 CONCLUSION

In the present work, the CFD simulations have been performed on centrifugal slurry pump, in order to obtain design improvements in the existing model of pump. CFD analysis of existing pump has been taken into consideration and new design modifications are suggested. Moreover, CFD simulation results of the suggested models are compared with the existing pump design. Certain other design parameters have also been considered in order to give additional design improvements. The results of the present work on the flow analysis of various designs yields following major conclusions:

- CFD simulation results were very useful in visualizing and understanding the complex flow inside the pump. After visualizing the previous CFD results certain areas for design improvement have been found.
- The recirculation flow around the cutwater region at lower flow rate was not travelling towards the belly region of the impeller smoothly. Also, tongue outlet was not carrying the flow properly.
- Discharge slope of the tongue was varied in order to improve the outlet flow. Two designs were obtained namely, Straight discharge tongue and Slanted discharge

tongue. It was found that the Straight Discharge Model is performing much better than the existing model and Slanted Discharge Model at 1450 rpm.

- In order to rectify irregular flow through cutwater region at low flow rates, cutwater was blended with constant radius of 5 mm. Two models were developed by rounding the cutwater region. Model 1 was made by rounding off the cutwater region of existing pump model and the Model 2 was made by rounding off the cutwater region of Straight Discharge Tongue model discussed in section 4.1.1. It has been found that Model 2 is performing better than the other two models. Also the flow near the cutwater in model 2, was smoother than other two models.
- Multiphase analysis of the improved design of the pump i.e. Model 2, has been done with bottom ash concentration 20% and 50%. It has been found that as the concentration of bottom ash increases the head decreases. Finally the plot for the Head Vs Flow rate was created for the Model 2.
- Two models were prepared with blade number 4 and 6 for analyzing the effect of blade number. CFD simulations for these two models were carried out for single phase (with water) at BEP. It has been found that, head for the 4 blade model is lower, than the other two models. But the head of the 6 blade is higher than the existing 5 blade model. So, the performance for higher blade number should also be tested and then an optimized number of blades should be considered.

6.2 FUTURE SCOPE

The present research work was aimed at improving the design of the existing model of centrifugal slurry pump using CFD. In order to improve the design process which been followed in the present work, there are several that can be augmented:

1. The blade numbers of the impeller can be optimized further for better design.
2. The prototypes of the discussed designs can be made using rapid prototyping process. And, the results obtained in the present work can be validated with the experimental results.
3. Other geometrical parameters such as: blade angle, blade width, impeller diameter etc. can be considered for further analysis.
4. Analysis of erosion wear can also be done.
5. The computerized codes for design such as Concepts- NREC's Pumpal, CFTurbo, and Turbo design can be integrated into the design process to shorten the design periods.

REFERENCES

1. Benretem, A., Haddouche, A., Cheghib, H. and Saad, S., (2007), Influence of Solid Particles on Centrifugal Pump Characteristics, *Journal of Engineering and Application Sciences*. v. 2, pp. 244-247.

2. Djerroud, M., "Numerical Identification of Key Design Parameters Enhancing the Centrifugal Pump Performance: Impeller, Impeller-Volute, and Impeller-Diffuser" International Scholarly Research Network, *ISRN Mechanical Engineering.* v. 11, pp.1-16

3. Grewal, H.S., Agrawal, A. and Singh, H., (2012), Design and Development of High-Velocity Slurry Erosion Test Rig Using CFD, *Journal of Materials Engineering and Performance.* v. 22, pp. 152–161

4. Hedi, L., Numerical Flow Simulation in a Centrifugal Pump, International Renewable Energy Congress, November 5-7, – Sousse, Tunisia.

5. Houlin, L., (2010), Effects of Blade Number on Characteristics of Centrifugal Pumps, *Chinese Journal Of Mechanical Engineering*. v.23, pp. 1-6.

6. Han, W., Ma, W., Li, R. N., Gao, Y. and Gao, H., (2012), Numerical Simulation of the Effect of Solid-Volume Fraction on Induction Force of Screw Centrifugal Pump, 26th Iahr Symposium on Hydraulic Machinery and Systems ,Iop Conf. Series: Earth And Environmental Science. v. 15, pp. 1-7.

7. Kumar, A., Kaushal, D.R. and Kumar, U., (2008), Bend Pressure Drop Experiments Compared with Fluent, Proceedings of The Institution of Civil Engineers Engineering and Computational Mechanics. v. 161, pp. 35–42.

8. Kaushal, D.R., Thinglas, T., Tomita, Y., Kuchii, S., Tsukamoto, H., (2012), CFD Modeling for Pipeline Flow of Fine Particles at High Concentration, *International Journal of Multiphase Flow*. v. 43, pp. 85–100.

9. Kumar, S. and Ratol, J.S., (2012), Experimental Investigation of Erosive Wear on the High Chrome Cast Iron Impeller of Slurry Disposal Pump using Response Surface Methodology, *Materials Engineering.* v. 19, pp. 110-116.

10. Liu, Y., Jiang, Y. and Han, Z.J., (2009), Research on the Pattern of Solid-Liquid Two-Phase Distribution in Chemical Process Pump, 26th IAHR Symposium on Hydraulic Machinery and Systems, Iop Conf. Series: Earth and Environmental Science. v.15, pp. 1-8.

11. Li, W.G.,(2011), Effect Of Exit Blade Angle, Viscosity And Roughness In Centrifugal Pumps Investigated By CFD Computation, *Task Quarterly.* v. 15, pp. 21–41.

12. Lipsett, M.G. and Bhushan, V., (2012), Modeling Erosion Wear Rates in Slurry Flotation Cells, *Journal of Fail. Anal. and Preven*. v. 12, pp. 51–65.

13. Liu, Y., Jiang, Y. and Han, Z.J., (2012), Research on the Pattern of Solid-Liquid Two-Phase Distribution in Chemical Process Pump, 26th Iahr Symposium on Hydraulic Machinery and Systems, *Earth and environmental science*. v. 15, pp. 1-8.

14. Ngoma, D.G., (2011), Numerical Identification of Key Design Parameters Enhancing the Centrifugal Pump Performance: Impeller, Impeller-Volute, and Impeller-Diffuser, International Scholarly Research Network , *ISRN Mechanical Engineering*. v. 2011, pp.1-16.

15. Pagalthivarthi, K.V., Gupta, P.K., Tyagi, V., Ravi, M.R., (2011), CFD Predictions of Dense Slurry Flow in Centrifugal Pump Casings, *International Journal of Aerospace and Mechanical Engineering*. v. 15, pp. 365-376.

16. Rababa, S.K., (2011), The Effect of Blades Number and Shape on the Operating Characteristics of Groundwater Centrifugal Pumps, *European Journal of Scientific Research.* v. 52 No.2, pp.243-251.

17. Rajendran, S., (2012), Analysis of a centrifugal pump impeller using ANSYS-CFX, *International Journal of Engineering Research & Technology*. v.1, pp. 1-6.

18. Singh, O.P., (2011), Parametric Study Of Centrifugal Fan Performance: Experiments And Numerical Simulation, *International Journal of Advances in Engineering & Technology*. v. 1, pp. 33-50.

19. Singh, R.R., (2012), Parametric Study And Optimization Of Centrifugal Pump Impeller By Varying The Design Parameter Using Computational Fluid Dynamics: Part I, Journal *of Mechanical and Production Engineering (JMPE).* v. 2, pp. 87-97.

20. Shojaeefard, M.H., (2012), Numerical study of the effects of some geometric characteristics of a centrifugal pump impeller that pumps a viscous fluid, *Computers & Fluids*. v. 60, pp. 61–70.

21. Singh, R.R., (2012), Optimizing Impeller Geometry For Performance Enhancement Of A Centrifugal Blower Using The Taguchi Quality Concept, *International Journal of Engineering Science and Technology (IJEST)*. v. 4, pp. 8-14.

22. Singh Sukhdeep,” Numerical Evaluation Of Flow Through A Centrifugal Slurry Pump Handling Bottom Ash & Fly Ash Using Cfd” M.E thesis, MED, T.U, Patiala, Punjab,2012.

23. Tang, X., Wang, F., Wu, Y., (2007), An Improved Large Eddy Simulation of Two-Phase Flows in a Pump Impeller, *Acta Mech Sin*. v. 23, pp. 635–643.

24. Wennberg**,** T., (2008), Predicting The Performance Of Centrifugal Pumps When Handling Complex Slurries, Proceedings 14th International Conference on Transport & Sedimentation of Solids particles. v. 14, pp. 324-333.

25. Wei, L., (2012), Analysis on Internal Solid-liquid Two-phase Flow in the Impellers of Sewage Pump, International Conference on Advances in Computational Modeling and Simulation,Procedia Engineering. v. 31, pp. 170 – 175.

26. Yang, D., Tan, Y., Zhang, H., Jiang, S., Song, J., sheng, Y., (2011), Numerical Simulation of Concrete Pumping Process and Investigation of Wear Mechanism of the Piping Wall, *Tribology International.* v. 46, pp.137-144.

27. Yi, L., Zuchao, Z., Weiqiang, H. and Zhaohui, H., (2012), Numerical Simulation and Experimental Research on the Influence of Solidphase Characteristics on Centrifugal Pump Performance, *Chinese Journal of Mechanical Engineering*. v. 25, pp. 1184-1189.

28. Yuliang, Z., Yi, L., Baoling, C., Zuchao , Z. and Huashu, D., (2013), Numerical Simulation and Analysis of Solid-liquid Two phase Flow in Centrifugal Pump, *Chinese Journal of Mechanical Engineering*. v. 26, pp. 53-60.

29. Zhao, B.J., Huang, Z.F., Chen, H.L. and Hou, D.H., (2012), Numerical Investigation of Solid-Liquid Two Phase Flow in a Non-Clogging Centrifugal Pump at Off-Design Conditions, 26th Iahr Symposium on Hydraulic Machinery and Systems, Iop Conference Series:Earth and environmental science. v. 15, pp. 620-640.